
UHR-Micro: Diagnosing and Mitigating the Resolution Illusion in Earth Observation VLMs

Shuo Ni^{1,3*}, Tong Wang^{1*}, Jing Zhang^{2,3†}, He Chen¹,
Haonan Guo^{3,4†}, Ning Zhang^{1,5†}, Bo Du^{2,3†}

¹National Key Laboratory of Science and Technology on Space-Born Intelligent Information Processing, Beijing Institute of Technology, Beijing, China

²School of Computer Science, Wuhan University, Wuhan, China

³Zhongguancun Academy, Beijing, China

⁴State Key Laboratory of Information Engineering in Surveying, Mapping and Remote Sensing, Wuhan University, Wuhan, China

⁵The Department of Computing, Hong Kong Polytechnic University, Hong Kong

shuoni@bit.edu.cn; jingzhang.cv@gmail.com

haonan.guo@whu.edu.cn; nzhang.rs@bit.edu.cn

dubo@whu.edu.cn

* Equal contribution. † Corresponding authors.

Abstract

Vision-Language Models (VLMs) increasingly operate on ultra-high-resolution (UHR) Earth observation imagery, yet they remain vulnerable to a severe scale mismatch between large-scale scene context and micro-scale targets. We refer to this empirical gap as a “resolution illusion”: higher input resolution provides the appearance of richer visual detail, but does not necessarily yield reliable perception of spatially small, task-relevant evidence. To benchmark this challenge, we introduce UHR-Micro, a benchmark comprising 11,253 instructions grounded in 1,212 UHR images, designed to evaluate VLMs at the spatial limits of native Earth observation imagery. UHR-Micro spans diverse micro-target scales, context requirements, task families, and visual conditions, and provides diagnostic annotations that support controlled evaluation and fine-grained error attribution. Experiments with representative high-resolution VLMs show substantial failures in spatial grounding and evidence parsing, despite access to high-resolution inputs. Further analysis suggests that these failures are not fully resolved by increasing model capacity, but are closely tied to insufficient guidance in locating and using task-relevant micro-evidence. Motivated by this finding, we propose Micro-evidence Active Perception (MAP), a reference agent that decomposes queries into evidence-seeking steps, actively inspects candidate regions, and grounds its answers in localized observations. MAP-Agent improves micro-level perception by making high-resolution reasoning evidence-centered rather than image-centered. Together, UHR-Micro and MAP-Agent provide a diagnostic platform for evaluating, understanding, and advancing high-resolution reasoning in Earth observation VLMs. Datasets and source code were released at [UHR-Micro](#).

1 Introduction

Recent advances in Vision-Language Models (VLMs) have substantially improved general visual understanding [42, 45]. Yet applying these models to Earth observation exposes a fundamental scale conflict between large geographic context and micro-targets [9, 24]. Ultra-high-resolution (UHR)

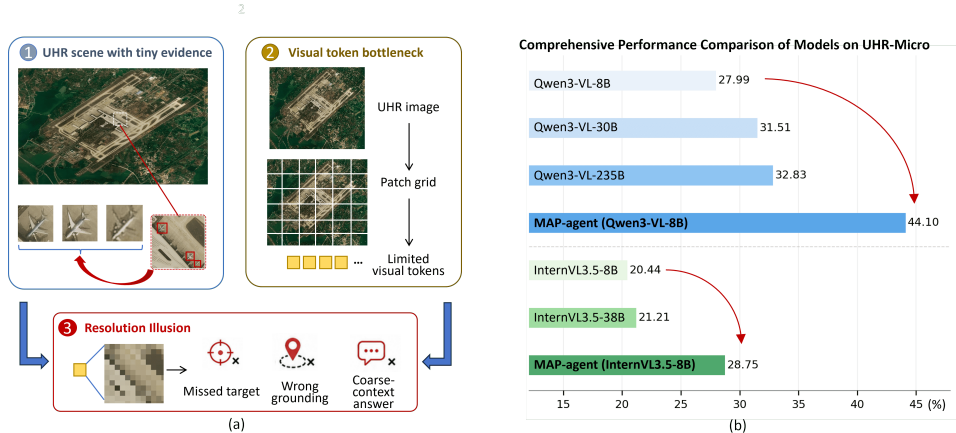


Figure 1: Resolution illusion and MAP-Agent performance gains. (a) UHR scenes may contain visually available but spatially tiny evidence that becomes inaccessible after token compression, leading VLMs to miss targets or rely on coarse context. (b) MAP-Agent addresses this failure mode through active micro-evidence localization, yielding substantial improvements over its backbone models on UHR-Micro.

remote sensing images often span broad scenes, while task-relevant evidence may occupy only a minuscule fraction of the pixels [32, 39]. Such evidence can include vehicles, vessels, small facilities, or narrow infrastructure [35]. This extreme scale disparity requires VLMs to preserve global scene context while performing precise micro-level perception [22].

Standard VLM pipelines are usually constrained by fixed visual token budgets. When UHR images are resized [15], patched [13], or compressed into a limited set of visual tokens [6], small visual cues can be weakened before reasoning begins [43, 27]. We refer to this empirical gap as a *resolution illusion*: higher nominal resolution suggests richer visual evidence, yet measured performance remains poor on tasks requiring spatially small evidence. In Earth observation, such failures can lead to missed targets, incorrect spatial grounding, or answers based on coarse scene context rather than localized observations, as shown in Fig. 1.

Existing remote sensing VLM benchmarks are not designed to isolate this failure mode. Most focus on image-level semantics [21, 11], salient objects [30, 41], or coarse scene understanding [23, 1, 2]. These tasks are valuable, but they do not test whether a model can locate and use micro-evidence embedded in large UHR scenes. They also offer limited diagnostic control over target scale, spatial distribution, context range, task family, and visual condition [18]. Without such diagnostic control, it is difficult to distinguish genuine micro-evidence grounding from answers driven by coarse visual context, language priors, or dataset shortcuts [8]. A dedicated benchmark is therefore needed to evaluate UHR reasoning at the level of task-relevant micro-evidence.

To address this gap, we introduce **UHR-Micro**, a benchmark for evaluating whether VLMs can locate, parse, and reason over task-relevant micro-evidence in UHR Earth observation imagery. UHR-Micro contains 11,253 instructions grounded in 1,212 curated UHR images, with task-relevant targets occupying less than 0.01% of the image area on average. These instructions span 16 tasks across diverse target scales, context requirements, visual conditions, and four task families: grounding, counting, spatial reasoning, and fine-grained understanding. Rather than evaluating only scene-level recognition, UHR-Micro centers each instruction on spatially small evidence that must be localized and used to answer the query. This design enables controlled evaluation of the gap between input resolution and effective micro-level perception.

UHR-Micro is constructed through a hybrid human-in-the-loop annotation process that enforces strict visual dependency. Each instruction is designed to require image-grounded evidence rather than language-only priors. Experiments on representative high-resolution VLMs reveal substantial failures in spatial grounding and evidence parsing, even when models have access to high-resolution inputs. Further analysis suggests that these failures are not fully resolved by increasing model capacity, but are closely tied to insufficient guidance in locating and using task-relevant micro-evidence.

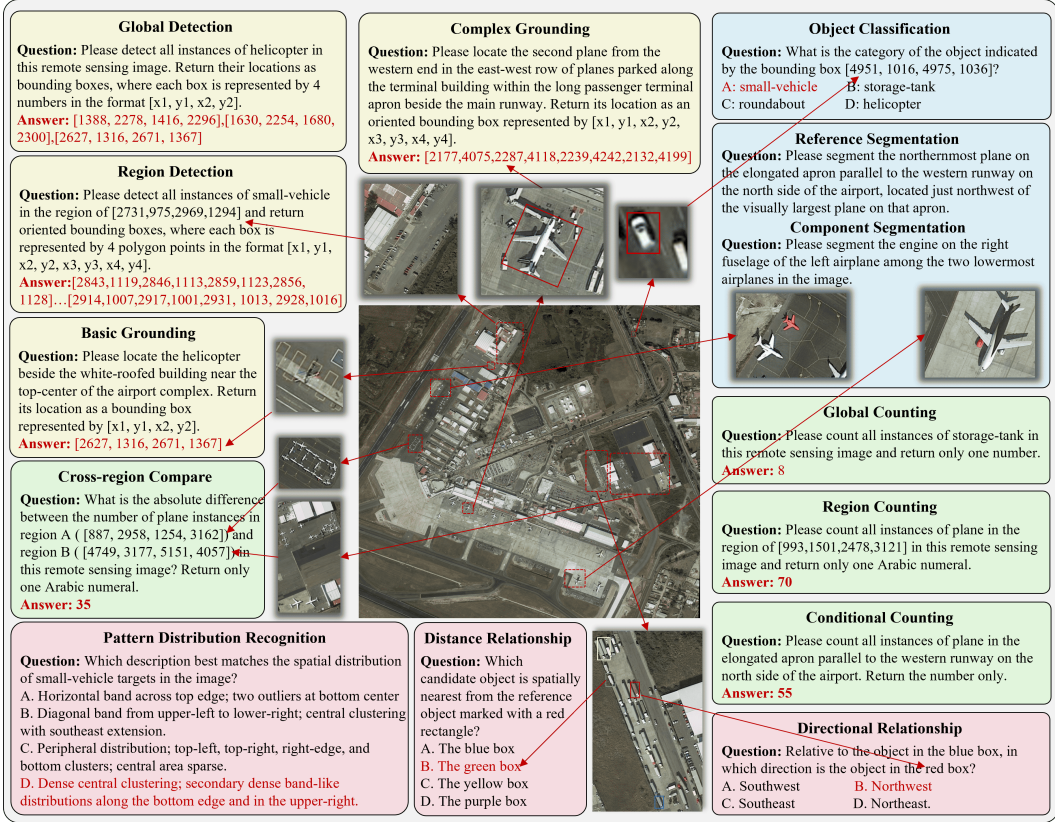


Figure 2: Overview of UHR-Micro. The benchmark evaluates micro-level perception in UHR Earth observation across grounding, fine-grained understanding, counting, and spatial reasoning. Each task is centered on spatially tiny evidence, forcing models to locate and use local observations rather than relying on coarse scene context.

Motivated by this finding, we propose **Micro-evidence Active Perception (MAP)**, a reference agent for evidence-centered high-resolution reasoning. MAP-Agent decomposes each query into evidence-seeking steps, actively inspects candidate regions, and grounds its answer in localized observations. This process guides the model to locate and verify task-relevant micro-evidence before producing an answer. Across two backbone baselines, MAP-Agent improves average performance on UHR-Micro by 12.2 points, suggesting that evidence-centered reasoning is an effective strategy for micro-level perception.

Our main contributions are summarized as follows:

- **UHR-Micro Benchmark.** We introduce UHR-Micro, a diagnostic benchmark of 11,253 instructions over 1,212 UHR Earth observation images, spanning 16 micro-evidence tasks with targets occupying less than 0.01% of the image area on average.
- **Resolution Illusion Analysis.** Experimental analysis on UHR-Micro operationalizes the *resolution illusion* as the gap between nominal high-resolution input access and measured micro-evidence grounding, with representative VLMs failing in spatial grounding and evidence parsing.
- **MAP-Agent.** MAP-Agent performs Micro-evidence Active Perception by decomposing queries into evidence-seeking steps, inspecting candidate regions, and grounding answers in localized observations, improving average UHR-Micro performance by 12.2 points across baseline VLMs.

2 Related Work

Multimodal Benchmarks in Earth Observation. Multimodal remote sensing evaluation initially centered on task-specific datasets, with RSVQA-HR [20] and RSVG [30] establishing paradigms

Table 1: Dataset statistics and comparison with representative vision-language benchmarks. RS denotes remote sensing, FF denotes free-form answers.

Dataset	Domain	Average Resolution	Average Target Size	Target Size Proportion	Volume	Output Type
MMBench [19]	General	512 × 270	-	-	3,217	Option
MMstar [5]	General	512 × 375	-	-	1,500	Option
RefCOCO [40]	General	640 × 480	70 × 70	1.59%	17,596	BBox
MME-Realworld [43]	General	2,000 × 1,500	-	-	29,429	Option
UCM-Caption [21]	RS	256 × 256	-	-	10,500	FF
RSVQA-HR [20]	RS	1,024 × 1,024	-	-	1,066,316	Option
RSVG [30]	RS	800 × 800	60 × 60	0.56%	7,933	BBox
DIOR-RSVG [41]	RS	800 × 800	170 × 170	4.52%	38,320	BBox
RRSIS-D [17]	RS	800 × 800	200 × 200	6.25%	17,402	Mask
LHRS-Bench [23]	RS	460 × 420	-	-	140,000	Option
Geochat-bench [11]	RS	630 × 620	120 × 120	3.69%	318,000	FF, BBox
CHOICE [1]	RS	650 × 650	160 × 130	4.92%	9,550	Option, BBox, Mask
VRSBench [2]	RS	512 × 512	120 × 120	5.49%	205,317	FF, BBox
XLRS-Bench [32]	RS	8,500 × 8,000	200 × 200	0.06%	45,942	FF, Option, BBox
UHR-Micro	RS	4,800 × 3,200	50 × 30	0.01%	11,253	Option, Number, BBox, Mask

for visual question answering and region grounding. The field has since moved toward broader instruction-following benchmarks: LHRS-Bench [23] introduced multi-granularity tasks, while VRSBench [2] targeted region-level visual comprehension at scale. Recent efforts further scale evaluation through zero-shot diagnostics in GEOBench-VLM [9] and globally distributed data in OmniEarth-Bench [31]. However, extremely small objects remain systematically underexplored. Existing benchmarks often rely on downsampling, cropped patches, or macro-level semantics even for large scenes [32], bypassing the severe scale disparity of native UHR imagery. UHR-Micro fills this gap by evaluating micro-level perception directly in UHR scenes.

Resolution Constraints and Perceptual Limitations. Fixed-resolution encoders such as CLIP [25] inevitably erase micro-features when resizing ultra-high-resolution imagery. Although recent models adopt dynamic strategies, including adaptive tiling in LLaVA-NeXT [13] and InternVL3.5 [37], or dynamic resolution encoding in Qwen3-VL [4], they still face fundamental perceptual bottlenecks. Minute object signals may be lost during token compression or overwhelmed by background noise, causing models to rely on linguistic priors and hallucinate [14]. UHR-Micro operationalizes this “resolution illusion” by measuring whether nominal high-resolution input access translates into effective micro-level perception.

Strategic Inference and Active Perception. Active perception has been explored to improve visual reasoning under limited visual budgets. DeepEyes [44] adaptively crops informative regions, enabling VLMs to inspect fine-grained details beyond a global view. In Earth observation, GeoEyes [34] and ZoomEarth [16] incorporate VLM agents, region selection, or iterative zooming for geospatial reasoning. These works demonstrate the value of zoom-based inspection for high-resolution understanding. MAP-Agent builds on this mechanism, but emphasizes discovering and aggregating localized micro-evidence for evidence-grounded reasoning.

3 UHR-Micro

3.1 Task Taxonomy for Micro-Level Perception

To comprehensively probe the perceptual limits of VLMs under extreme scale disparities, we construct a multi-dimensional evaluation taxonomy anchored by four pillars. Each dimension isolates a fundamental facet of visual perception. Together, they systematically evaluate not only where and what the micro-targets are, but also how many exist and how they spatially relate across the macroscopic canvas, providing a holistic assessment of micro-level perception.

Grounding. Focused on spatial anchoring, this dimension evaluates the model’s ability to locate micro-targets amid vast backgrounds through five tasks. *Global Detection (GD)* requires open-ended search over the entire image, while *Regional Detection (RD)* restricts detection to bounded sub-areas. *Basic Grounding (BG)* identifies unique targets from simple spatial cues without similar distractors, whereas *Complex Grounding (CG)* requires multi-step or multi-hop reasoning over spatial and relational cues, such as exact ordinal positioning within dense clusters. *Multi-Condition Retrieval (MCR)* further asks models to retrieve all targets satisfying combined textual attributes and spatial relations.

Fine-grained Understanding. Beyond localization, fine-grained understanding examines whether models can capture semantic and morphological details of micro-targets. *Object Classification (OC)* tests basic category assignment for extremely small instances. *Fine-Grained Recognition (FGR)* requires identifying specific subtypes, such as aircraft or ship models. At the pixel level, *Referring Segmentation (RS)* is evaluated against object masks specified by textual descriptions, while *Component Segmentation (CS)* is evaluated against masks of tiny components such as aircraft empennages.

Counting. For numerical perception, UHR-Micro evaluates models on dense micro-target enumeration through four tasks. *Global Counting (GC)* and *Regional Counting (RC)* require exhaustive counting over the full image and bounded regions, respectively. *Conditional Counting (CC)* introduces semantic constraints by counting targets with specified visual attributes. *Cross-Region Compare (CRC)* further requires tracking disjoint spatial regions and computing numerical differences between their target populations.

Spatial Reasoning. To assess geometric and topological awareness, we include three spatial reasoning tasks over micro-targets. *Directional Relationship (DrR)* and *Distance Relationship (DsR)* test local pairwise spatial relations, while *Pattern Distribution Recognition (PDR)* examines global distribution patterns and object-swarm topology.

To avoid subjective bias, all tasks are unified into four deterministic output formats: bounding boxes, segmentation masks, exact numbers, and discrete options. This design ensures that the benchmark remains unambiguous, quantitative, and fully reproducible.

3.2 Data Engine and Annotation

UHR-Micro contains 1,212 curated images from established remote sensing datasets, including FAIR1Mv2 [29], DOTA v2 [38], SODA-A [22], and xView [12]. To ensure extreme scale disparities, almost all selected images exceed 4,000 pixels along the long edge. Built on this UHR foundation, we design a three-tier hybrid data engine to balance scale and annotation quality. First, foundational tasks driven by coordinate or category mapping, such as *GD*, *OC*, and spatial relations, are programmatically generated from dense ground-truth annotations via geometric rules. Second, tasks requiring descriptive semantic alignment, including *BG* and *PDR*, are generated by a frontier VLM and then cross-validated by human annotators. Third, tasks involving deep reasoning, such as *CG*, *CRC*, and *MCR*, are led by domain experts with model assistance and rigorous expert review. This pipeline scales the annotation process while preserving objective evaluation. All generated instructions are subjected to manual verification or rule-based consistency checks before inclusion. Detailed rules, prompts, and protocols are provided in the Appendix.

3.3 Analysis

UHR-Micro includes 11,253 deterministic evaluation instructions distributed across the 16 tasks. The instruction pool is partitioned into development, validation, and test splits. In our experiments, validation is used only for prompt-format checking and inference-protocol selection, while test is reserved for final benchmarking. Tab. 1 compares UHR-Micro with existing vision-language datasets. UHR-Micro uniquely couples UHR imagery with extreme micro-targets: although the average long-edge resolution exceeds 4,000 pixels, target sizes and their relative proportions remain exceptionally small. This severe spatial disparity is designed to isolate micro-level visual extraction and reduce reliance on linguistic priors.

4 Findings and Baseline

To systematically address the challenges posed by the UHR-Micro benchmark, we first conduct a pilot study to analyze the behavior of representative VLMs under different visual perception strategies. The insights derived from this analysis directly motivate the design of our active perception agent.

4.1 Pilot Study and Empirical Findings

We evaluated two representative models, Qwen3-VL-8B [4] and GPT-5.2 [28], on the UHR-Micro validation split. To isolate the impact of spatial resolution and localization strategies, we implement

Table 2: Performance on the UHR-Micro validation split for Qwen3-VL-8B [4] and GPT-5.2 [28] under different UHR perception strategies. Scores are percentages. Dashes denote strategy-task pairs where no separate score is reported; when computing Avg.[†], these entries are filled with the corresponding Native score of the same model and task to preserve a common task distribution.

Model	Strategy	Grounding				Fine-grained Understanding				Counting			Spatial Reasoning			Avg. [†]		
		GD	RD	BG	CG	MCR	OC	FGR	RS	CS	GC	RC	CC	CRC	DrR		DsR	PDR
Qwen3-VL-8B [4]	Native	23.64	3.76	34.41	16.76	24.62	52	26	26.63	22.69	34.76	5.73	28.19	13.10	49	70	78	31.83
	Resize-1024	12.47	0.48	18.39	10.52	15.13	53	27	16.90	18.61	15.14	3.52	25.51	12.56	38	52	69	24.26
	Query Crop	-	59.52	-	-	-	55	32	-	-	-	49.72	-	-	-	-	-	38.63
	Oracle GT-Crop-512	-	19.87	59.62	66.18	-	83	35	64.54	51.38	-	36.05	-	-	-	-	-	46.06
	Oracle GT-Crop-1024	-	43.35	56.15	43.40	-	75	32	61.49	45.28	-	56.45	-	-	-	-	-	45.90
	Oracle GT-Crop-2048	-	0.93	44.34	25.56	-	66	27	46.72	40.18	-	4.95	-	-	-	-	-	36.06
Sliding Window-1024	28.67	2.19	7.87	1.30	13.24	56	18	22.31	13.41	38.13	22.62	25.00	-	-	-	-	28.68	
GPT-5.2 [28]	Native	9.90	6.45	3.91	2.76	14.46	52	25	4.86	3.16	35.64	15.00	24.30	22.00	47	43	76	24.09
	Resize-1024	8.76	8.47	5.19	2.88	14.67	46	21	8.35	4.54	24.32	12.93	24.45	17.39	55	40	73	22.93
	Query Crop	-	37.96	-	-	-	59	29	-	-	-	55.20	-	-	-	-	-	29.26
	Oracle GT-Crop-512	-	46.30	48.78	48.23	-	84	27	55.84	33.92	-	54.01	-	-	-	-	-	41.90
	Oracle GT-Crop-1024	-	41.68	29.09	28.97	-	80	31	34.60	21.02	-	59.31	-	-	-	-	-	37.37
	Oracle GT-Crop-2048	-	16.60	12.33	6.62	-	65	30	12.99	7.23	-	36.89	-	-	-	-	-	28.75
Sliding Window-1024	40.29	39.77	11.07	6.72	28.87	56	26	-	-	44.90	54.16	20.15	-	-	-	-	32.75	

five comparative settings: 1) **Native**: Direct input of the original UHR image without external resizing or cropping; 2) **Resize**: Down-sampling the global image to 1024 pixels; 3) **Query Crop**: For tasks with explicit coordinate prompts, directly cropping the designated region; 4) **Oracle GT-Crop**: Cropping regions centered around the ground-truth targets at varying window sizes; and 5) **Sliding Window**: An exhaustive traversal of the global image using fixed-size patches.

Summarized in Tab. 2, the quantitative results reveal three critical findings regarding micro-target perception:

Finding 1: Scale disparity outweighs absolute resolution. Performance generally decreases in the Resize-1024 setting compared to the Native setting, with the degradation especially pronounced for Qwen3-VL-8B [4]. This confirms that the primary bottleneck in UHR understanding is not merely the large grid size, but the extreme relative proportion of micro-targets. Downsampling removes critical details before the VLM can process the image.

Finding 2: VLMs can recognize micro-targets once localized evidence is provided. Both the Query Crop and Oracle GT-Crop strategies yield substantial gains over the Native setting, indicating that poor native performance is not solely caused by a lack of fine-grained recognition ability. Instead, much of the difficulty lies in finding the task-relevant evidence within the massive image canvas. Once localized, original-resolution crops are provided, VLMs can better exploit their latent recognition capability. Further evaluation under the Oracle GT-Crop setting shows that crop windows of 512 and 1024 pixels achieve optimal performance, while expanding the window to 2048 pixels causes a noticeable drop. This suggests that excessively large receptive fields reintroduce background noise and dilute micro-target features.

Finding 3: The prohibitive cost of blind search. While the Sliding Window strategy passively guarantees native-resolution coverage and improves metric performance in some tasks, it incurs unacceptable computational overhead. Specifically, this exhaustive strategy requires an average of 29.8 model calls per question, drastically inflating the computational cost for each image. Such redundancy renders sliding windows impractical for real-world UHR deployment.

Driven by these empirical insights, a practical UHR perception system should decouple macroscopic search from fine-grained recognition. Since VLMs can recognize micro-targets when localized evidence is available, the key challenge becomes how to identify informative regions efficiently. This motivates a shift toward dynamic localization, where task-relevant regions are selectively discovered before fine-grained inspection and final reasoning.

4.2 MAP-Agent

Following this design principle, **MAP-Agent** operationalizes evidence-centered high-resolution reasoning with a three-stage pipeline, as illustrated in Fig. 3. The pipeline consists of query-guided evidence discovery, localized evidence inspection, and global-local evidence synthesis. Together, these stages guide the model to search for task-relevant micro-evidence, inspect candidate regions, and ground the final answer in localized observations.

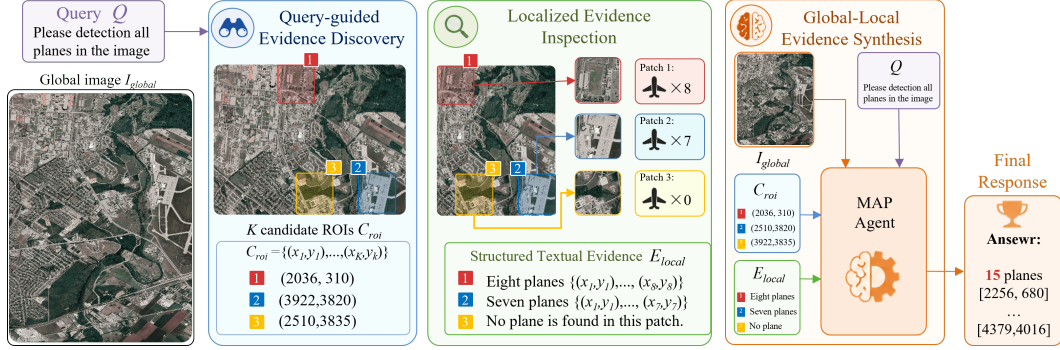


Figure 3: MAP-Agent pipeline for evidence-centered UHR reasoning. MAP-Agent first discovers query-relevant candidate regions, then inspects localized original-resolution crops, and finally synthesizes global context with local evidence. This process converts UHR perception from passive image understanding into active micro-evidence seeking.

Query-guided Evidence Discovery. Given the input query Q and the global image I_{global} , the first stage searches for candidate regions that may contain task-relevant micro-evidence. Instead of traversing the entire image with dense sliding windows, the agent uses the query semantics and global scene layout to predict a compact set of K region-of-interest anchor points, denoted as $C_{roi} = \{c_i\}_{i=1}^K$, where each $c_i = (x_i, y_i)$ specifies a point location in the coordinate system of the original UHR image. This stage does not aim to answer the question directly. Its role is to provide evidence-seeking anchors that guide the subsequent local inspection toward regions with high relevance to the query.

Localized Evidence Inspection. Given each candidate anchor point $c_i \in C_{roi}$, MAP-Agent extracts a local patch of window size $S \times S$ centered at c_i from the original UHR image and inspects it for fine-grained and query-relevant details. The local inspection focuses on micro-level observations such as object presence, counts, attributes, positions, or spatial relations. These observations are associated with their corresponding image locations and converted into structured textual evidence, denoted as $E_{local} = \{e_i\}_{i=1}^K$. In this stage, cropped regions are treated as sources of localized micro-evidence rather than as independent inputs for immediate final prediction.

Global-Local Evidence Synthesis. The final stage combines global scene context with localized evidence collected from candidate regions. Given the query Q , the global image I_{global} , the candidate anchors C_{roi} , and the local evidence E_{local} , the agent reasons over both the macroscopic scene layout and the micro-level observations extracted from local patches. The global image provides contextual information such as scene structure, object arrangement, and coarse spatial relations, while E_{local} supplies fine-grained evidence that may be difficult to preserve in a global visual representation alone. By anchoring localized observations back to their positions in the full image, MAP-Agent produces an answer grounded in both global context and task-relevant micro-evidence.

5 Experiment

5.1 Experimental Setup

Following the held-out split described above, all final results are reported on the test split of UHR-Micro. The validation split is used only for inference-time protocol selection, such as the number of candidate regions and crop size, and no model weights are updated. Based on validation performance, MAP-Agent uses a $S = 1024$ crop window with task-adaptive ROI allocation: global search and multi-condition retrieval tasks use a larger ROI budget, and other tasks use a smaller default budget. These settings are fixed before test evaluation. We evaluate four groups of models. The first group contains open-source general-purpose VLMs, including Qwen2-VL-7B [36], Qwen2.5-VL-7B [10], Qwen3-VL-8B [4], Qwen3-VL-30B, Qwen3-VL-235B, InternVL3.5-8B [37], and InternVL3.5-38B. The second group contains closed-source frontier VLMs, including GPT-5.2 [28], Gemini-2.5-Pro [7], and Claude 3.7 Sonnet [3]. The third group contains remote-sensing-oriented VLMs and geospatial agents, including DeepEyes [44], GeoChat [11], GeoLLaVA-8K [33], and GeoEyes [34]. The fourth

Table 3: Performance on the UHR-Micro test split for representative models and MAP-Agent variants. Scores are reported as percentages. Category-level Avg. columns average the tasks within each category, while the final Avg. column averages all 16 task scores. The best and second-best results in each column are marked in bold and underlined, respectively.

Model	Grounding						Fine-grained Understanding					Counting					Spatial Reasoning				Avg.
	GD	RD	BG	CG	MCR	Avg.	OC	FGR	RS	CS	Avg.	GC	RC	CC	CRC	Avg.	DrR	DsR	PDR	Avg.	
Qwen2-VL-7B [36]	0.18	0.46	0.34	0.03	0.01	0.21	50.94	25.89	10.56	5.01	23.10	23.83	14.08	35.05	18.38	22.84	46.25	32.08	45.51	41.61	19.35
Qwen2.5-VL-7B [10]	1.06	0.63	0.53	1.16	2.01	1.08	58.83	30.05	10.25	7.05	26.55	30.59	18.22	37.34	27.96	28.53	64.78	42.14	63.95	56.96	24.78
Qwen3-VL-8B [4]	6.76	0.27	15.07	5.41	4.05	6.31	51.97	31.09	13.94	4.60	25.40	25.94	5.34	27.59	21.10	19.99	77.50	72.33	<u>84.89</u>	78.24	27.99
Qwen3-VL-30B [4]	12.07	3.83	17.51	8.50	11.05	10.59	51.97	30.96	23.86	10.67	29.37	29.39	5.62	31.82	25.30	23.03	<u>82.50</u>	<u>74.84</u>	<u>84.30</u>	<u>80.55</u>	31.51
Qwen3-VL-235B [4]	12.39	1.74	<u>19.60</u>	10.64	11.88	11.25	55.06	36.55	27.00	8.95	31.89	33.78	4.39	23.92	18.23	20.08	92.50	76.73	91.86	87.03	32.83
InternVL3.5-8B [37]	1.87	0.15	5.34	1.31	0.51	1.83	49.06	25.38	13.96	4.58	23.24	19.40	10.90	46.50	19.60	24.10	28.00	37.11	63.37	42.83	20.44
InternVL3.5-38B [37]	1.70	0.05	12.69	3.29	0.97	3.74	54.37	28.93	22.90	4.80	27.75	3.46	7.40	12.53	13.90	9.32	42.50	49.68	80.23	57.47	21.21
GPT-5.2 [28]	2.33	7.61	4.24	3.52	1.85	3.91	50.09	30.96	5.74	1.83	22.16	33.67	14.07	23.49	25.63	24.21	57.50	52.20	81.40	63.70	24.76
Gemini-2.5-Pro [7]	8.24	26.47	7.65	4.10	11.36	<u>11.56</u>	55.57	35.53	4.93	2.00	24.51	28.83	33.50	32.22	20.60	28.79	55.95	53.76	58.72	56.14	27.46
Claude 3.7 Sonnet [3]	5.11	<u>26.54</u>	1.83	0.52	5.25	9.85	26.59	30.46	3.13	3.39	15.89	19.88	2.81	27.61	3.23	13.38	31.73	30.93	16.86	26.51	15.37
DeepEyes [44]	4.23	9.17	3.30	2.55	6.76	5.20	57.12	29.44	2.37	2.54	22.87	37.88	29.24	40.03	<u>26.84</u>	<u>33.50</u>	56.88	42.77	65.12	54.92	26.01
GeoChat [11]	1.59	1.74	1.58	0.51	4.60	2.00	47.17	26.90	4.79	3.28	20.54	22.88	14.45	51.55	24.59	28.37	28.13	21.70	19.19	23.00	17.17
GeoLaVa-8k [33]	0.52	0.00	0.00	0.00	0.00	0.10	30.53	30.96	0.00	0.00	15.37	0.00	0.19	2.16	0.00	0.59	23.13	24.53	29.65	25.77	8.85
GeoEyes [34]	0.11	0.62	0.26	0.21	0.50	0.34	1.72	0.00	1.18	1.71	1.15	3.13	0.71	0.00	4.84	2.17	63.43	41.56	32.56	45.85	9.53
MAP-Agent (InternVL3.5-8B)	6.41	5.15	14.99	<u>11.99</u>	<u>16.58</u>	11.02	<u>62.09</u>	30.96	18.40	<u>10.92</u>	30.59	<u>38.42</u>	45.94	35.46	26.35	36.54	44.38	31.45	60.47	45.43	28.75
MAP-Agent (Qwen3-VL-8B)	29.79	64.46	37.01	23.92	23.55	35.75	64.32	38.07	41.29	17.86	40.38	40.98	<u>43.29</u>	29.59	17.98	32.96	76.25	73.58	83.72	77.85	44.10

group contains MAP-Agent variants built on top of the Qwen3-VL-8B and InternVL3.5-8B baselines. All models are evaluated on the same image-query pairs, with coordinate outputs converted to absolute pixels for scoring; we use a 1000-base protocol by default and model-native protocols when specified. For segmentation tasks, we use a standardized box-to-mask protocol: models first predict bounding boxes, which are then converted to absolute pixels and used as SAM2 [26] box prompts for mask generation. Additional implementation details are provided in the Appendix.

5.2 Evaluation Metrics

UHR-Micro contains heterogeneous answer formats, including categorical choices, counts, box localization, multi-region detection, and segmentation. We normalize all task scores to $[0, 1]$, multiply them by 100 for reporting, and compute the overall score as the macro-average over tasks. Empty, invalid, or unparseable predictions are assigned zero.

For categorical tasks, we use exact accuracy after normalizing model outputs to canonical labels. For counting tasks, we use a bounded relative counting score rather than exact match, so that errors are penalized according to their magnitude relative to the ground-truth count. For single-target localization, we use a continuous localization score that combines box overlap with center proximity, avoiding brittle hard-threshold matching for micro-scale targets. For multi-region detection and retrieval, ground-truth and predicted boxes are greedily matched, and the final score is computed as a soft F1 over matched localization scores. For segmentation tasks, we use the same continuous formulation with mask IoU replacing box IoU. Detailed metric definitions are provided in Appendix.

5.3 Main Results

Tab. 3 reports the main results on the UHR-Micro test split. A clear pattern is the separation between scene-level reasoning and micro-evidence grounding. Strong VLMs often perform well on spatial reasoning by exploiting global layouts and coarse relational priors. For instance, Qwen3-VL-235B [4] reaches 87.03 on spatial reasoning, yet its grounding average remains only 11.25. Such a gap would be obscured in conventional scene-level benchmarks, highlighting the diagnostic value of UHR-Micro.

Scaling and domain specialization only partially alleviate this bottleneck. Within the Qwen3-VL family, the overall score rises from 27.99 for Qwen3-VL-8B [4] to 32.83 for Qwen3-VL-235B [4], but grounding remains low even for the largest model. Closed-source frontier models show similarly uneven behavior: Gemini-2.5-Pro [7] obtains the second grounding average of 11.56, while GPT-5.2 [28] and Claude 3.7 Sonnet [3] are competitive only on selected categories. Remote-sensing-oriented models and geospatial agents remain limited, suggesting that, among evaluated models, domain knowledge alone is insufficient for micro-evidence localization.

MAP-Agent directly targets this weakness. Built on Qwen3-VL-8B [4], it improves the overall score from 27.99 to 44.10, surpassing the strongest non-MAP model by 11.27 points. Gains in fine-grained understanding and counting show that localized observations also benefit evidence-dependent

recognition and enumeration. The same trend holds for InternVL3.5-8B [37], where MAP-Agent improves the overall score by 8.31 points.

Overall, current VLMs are not uniformly weak in visual reasoning, but suffer from a specific bottleneck in accessing and using micro-evidence. Higher input resolution, larger capacity, and remote-sensing specialization provide limited gains, whereas MAP-Agent shifts UHR reasoning from image-centered perception toward evidence-centered reasoning.

5.4 Diagnostic Analysis

To better understand failure modes in micro-evidence grounding, we conduct a post-hoc error diagnosis on the complex grounding task in the UHR-Micro test split. We analyze the predictions of GPT-5.2 [28], Qwen3-VL-8B [4], and MAP-Agent based on Qwen3-VL-8B. Each prediction is assigned to one diagnostic category following a fixed priority order. Diagnostic labels are assigned by rule-based checks where possible and manually verified for ambiguous cases. We first check whether the output follows the required localization format. For valid boxes, we then examine whether the prediction falls inside the annotated semantic region, overlaps any valid object, confuses the object category, selects another instance of the correct category under the wrong contextual condition, or localizes the correct target with insufficient coordinate accuracy. Predictions with $\text{IoU} \geq 0.3$ to the ground-truth target are counted as successful cases, while unresolved failures are grouped into Other.

As shown in Tab. 4, MAP-Agent improves the success rate from 6.9% to 16.8% over the baseline. The improvement is accompanied by lower object hallucination, category hallucination, context hallucination, and coordinate shift, suggesting that multi-step evidence seeking helps verify localized micro-targets before final localization. Region hallucination remains the dominant residual error, highlighting the persistent difficulty of reliable global-to-local region selection.

Table 4: Error diagnosis on the *CG* task of the UHR-Micro test split. All entries are percentages. IF, RH, OH, CatH, CtxH, CS, Oth., and Succ. denote invalid format, region hallucination, object hallucination, category hallucination, context hallucination, coordinate shift, other failures, and $\text{IoU} \geq 0.3$ success, respectively.

Model	IF	RH	OH	CatH	CtxH	CS	Oth.	Succ.
GPT-5.2 [28]	1.6	60.9	25.1	4.5	4.5	2.1	1.3	0
Qwen3-VL-8B [4]	2.1	30.3	5.5	20.4	25.6	5.3	4.0	6.9
MAP-Agent	0.3	33.2	3.9	19.0	23.5	1.9	1.3	16.8

5.5 Ablation Study

We ablate two MAP-Agent inference factors using Qwen3-VL-8B [4] on the UHR-Micro validation split: crop window size and ROI allocation policy. For crop size, we compare $S = 512$ and $S = 1024$. For ROI allocation, we compare a task-adaptive policy with three uniform policies. The task-adaptive policy assigns more ROIs to global and multi-target queries, skips additional cropping for explicit-region queries, and uses a smaller default ROI budget otherwise. Uniform policies use the same number of ROIs for all non-explicit-region tasks.

As shown in Tab. 5, $S = 1024$ consistently improves overall performance over $S = 512$, especially in grounding and ROI hit rate, indicating the importance of sufficient local context. ROI allocation presents a clear performance–cost trade-off. Under $S = 1024$, Uniform-4 attains the highest ROI hit rate but requires more calls and does not improve the overall score, while Uniform-1 reduces cost but weakens grounding. The task-adaptive policy achieves the best overall score of 43.88 with moderate cost. We therefore adopt $S = 1024$ with task-adaptive ROI allocation as the default MAP-Agent configuration.

Table 5: Ablation of MAP-Agent crop size and ROI allocation on the UHR-Micro validation split. Und., Cnt., Grd., and Rel. denote understanding, counting, grounding, and relationship reasoning, respectively.

Config.	Und.	Cnt.	Grd.	Rel.	Avg.	ROI hit	Calls/QA
<i>1024 × 1024 crop window</i>							
Task-adaptive	42.17	35.84	36.01	70.00	43.88	59.5	3.53
Uniform-4	41.00	35.65	36.06	69.00	43.37	66.0	4.81
Uniform-2	42.18	36.10	35.42	70.00	43.76	62.0	3.59
Uniform-1	42.49	35.73	34.62	70.00	43.50	59.5	3.11
<i>512 × 512 crop window</i>							
Task-adaptive	41.81	34.83	34.65	69.67	43.05	44.5	3.67
Uniform-4	41.64	35.08	34.22	70.00	43.00	47.0	5.01
Uniform-2	41.81	34.62	34.07	69.33	42.76	45.0	3.72
Uniform-1	40.90	34.86	33.77	69.67	42.56	44.5	3.21

6 Conclusion

In this work, we presented UHR-Micro, a diagnostic benchmark for testing whether vision-language models can move beyond nominal high-resolution input access to truly locate and reason over micro-

scale evidence in ultra-high-resolution Earth observation imagery. UHR-Micro centers each query on spatially small yet task-critical visual evidence, covering 11,253 instructions across 1,212 UHR images and 16 tasks, with task-relevant targets occupying less than 0.01% of the image area on average. Our evaluation shows that, for the models studied, higher input resolution, larger model scale, and remote-sensing specialization do not necessarily translate into reliable micro-level perception. To mitigate this bottleneck, we introduced MAP-Agent, an evidence-centered reference strategy that decomposes queries, actively inspects candidate regions, and grounds answers in localized observations, improving average performance by 12.2 points across two backbone VLMs. These gains suggest that micro-level reasoning requires not only more pixels, but also better procedures for discovering and verifying task-relevant visual evidence. Nevertheless, residual errors such as region hallucination indicate that robust global-to-local grounding remains an open challenge. We hope UHR-Micro will support future research on perception-aware VLMs that can reason reliably at the spatial limits of real-world UHR imagery.

References

- [1] Xiao An, Jiaying Sun, Zihan Gui, and Wei He. Choice: benchmarking the remote sensing capabilities of large vision-language models. *Advances in Neural Information Processing Systems*, 38, 2026.
- [2] Xiao An, Jiaying Sun, Zihan Gui, and Wei He. Choice: benchmarking the remote sensing capabilities of large vision-language models. *Advances in Neural Information Processing Systems*, 38, 2026.
- [3] Anthropic. Claude 3.7 sonnet, 2025. URL <https://www.anthropic.com/news/claude-3-7-sonnet>.
- [4] Shuai Bai, Yuxuan Cai, Ruizhe Chen, Keqin Chen, Xionghui Chen, Zesen Cheng, Lianghao Deng, Wei Ding, Chang Gao, Chunjiang Ge, et al. Qwen3-vl technical report. *arXiv preprint arXiv:2511.21631*, 2025.
- [5] Lin Chen, Jinsong Li, Xiaoyi Dong, Pan Zhang, Yuhang Zang, Zehui Chen, Haodong Duan, Jiaqi Wang, Yu Qiao, Dahua Lin, et al. Are we on the right way for evaluating large vision-language models? *Advances in Neural Information Processing Systems*, 37:27056–27087, 2024.
- [6] Zhe Chen, Jiannan Wu, Wenhai Wang, Weijie Su, Guo Chen, Sen Xing, Muyan Zhong, Qinglong Zhang, Xizhou Zhu, Lewei Lu, et al. Internvl: Scaling up vision foundation models and aligning for generic visual-linguistic tasks. In *Proceedings of the IEEE/CVF conference on computer vision and pattern recognition*, pages 24185–24198, 2024.
- [7] Gheorghe Comanici, Eric Bieber, Mike Schaekermann, Ice Pasupat, Noveen Sachdeva, Inderjit Dhillon, Marcel Blistein, Ori Ram, Dan Zhang, Evan Rosen, et al. Gemini 2.5: Pushing the frontier with advanced reasoning, multimodality, long context, and next generation agentic capabilities. *arXiv preprint arXiv:2507.06261*, 2025.
- [8] Yunkai Dang, Meiyi Zhu, Donghao Wang, Yizhuo Zhang, Jiacheng Yang, Qi Fan, Yuekun Yang, Wenbin Li, Feng Miao, and Yang Gao. A benchmark for ultra-high-resolution remote sensing mllms. *arXiv preprint arXiv:2512.17319*, 2025.
- [9] Muhammad Danish, Muhammad Akhtar Munir, Syed Roshan Ali Shah, Kartik Kuckreja, Fahad Shahbaz Khan, Paolo Fraccaro, Alexandre Lacoste, and Salman Khan. Geobench-vlm: Benchmarking vision-language models for geospatial tasks. In *Proceedings of the IEEE/CVF International Conference on Computer Vision*, pages 7132–7142, 2025.
- [10] Binyuan Hui, Jian Yang, Zeyu Cui, Jiayi Yang, Dayiheng Liu, Lei Zhang, Tianyu Liu, Jiajun Zhang, Bowen Yu, Keming Lu, et al. Qwen2. 5-coder technical report. *arXiv preprint arXiv:2409.12186*, 2024.
- [11] Kartik Kuckreja, Muhammad Sohail Danish, Muzammal Naseer, Abhijit Das, Salman Khan, and Fahad Shahbaz Khan. Geochat: Grounded large vision-language model for remote sensing. In *Proceedings of the IEEE/CVF conference on computer vision and pattern recognition*, pages 27831–27840, 2024.
- [12] Darius Lam, Richard Kuzma, Kevin McGee, Samuel Dooley, Michael Laielli, Matthew Klaric, Yaroslav Bulatov, and Brendan McCord. xview: Objects in context in overhead imagery. *arXiv preprint arXiv:1802.07856*, 2018.
- [13] Feng Li, Renrui Zhang, Hao Zhang, Yuanhan Zhang, Bo Li, Wei Li, Zejun Ma, and Chunyuan Li. Llava-next-interleave: Tackling multi-image, video, and 3d in large multimodal models. *arXiv preprint arXiv:2407.07895*, 2024.

- [14] Yifan Li, Yifan Du, Kun Zhou, Jinpeng Wang, Xin Zhao, and Ji-Rong Wen. Evaluating object hallucination in large vision-language models. In *Proceedings of the 2023 conference on empirical methods in natural language processing*, pages 292–305, 2023.
- [15] Haotian Liu, Chunyuan Li, Yuheng Li, and Yong Jae Lee. Improved baselines with visual instruction tuning. In *Proceedings of the IEEE/CVF conference on computer vision and pattern recognition*, pages 26296–26306, 2024.
- [16] Ruixun Liu, Bowen Fu, Jiayi Song, Kaiyu Li, Wanchen Li, Lanxuan Xue, Hui Qiao, Weizhan Zhang, Deyu Meng, and Xiangyong Cao. Zoomearth: Active perception for ultra-high-resolution geospatial vision-language tasks. *arXiv preprint arXiv:2511.12267*, 2025.
- [17] Sihan Liu, Yiwei Ma, Xiaoqing Zhang, Haowei Wang, Jiayi Ji, Xiaoshuai Sun, and Rongrong Ji. Rotated multi-scale interaction network for referring remote sensing image segmentation. In *Proceedings of the IEEE/CVF Conference on Computer Vision and Pattern Recognition*, pages 26658–26668, 2024.
- [18] Yi Liu, Jing Zhang, Di Wang, Xiaoyu Tian, Haonan Guo, and Bo Du. Seeing clearly without training: Mitigating hallucinations in multimodal llms for remote sensing. *arXiv preprint arXiv:2603.02754*, 2026.
- [19] Yuan Liu, Haodong Duan, Yuanhan Zhang, Bo Li, Songyang Zhang, Wangbo Zhao, Yike Yuan, Jiaqi Wang, Conghui He, Ziwei Liu, et al. Mmbench: Is your multi-modal model an all-around player? In *European conference on computer vision*, pages 216–233. Springer, 2024.
- [20] Sylvain Lobry, Diego Marcos, Jesse Murray, and Devis Tuia. Rsvqa: Visual question answering for remote sensing data. *IEEE Transactions on Geoscience and Remote Sensing*, 58(12):8555–8566, 2020.
- [21] Xiaoqiang Lu, Binqiang Wang, Xiangtao Zheng, and Xuelong Li. Exploring models and data for remote sensing image caption generation. *IEEE Transactions on Geoscience and Remote Sensing*, 56(4):2183–2195, 2017.
- [22] Aref Miri Rekavandi, Shima Rashidi, Farid Boussaid, Stephen Hoefs, Emre Akbas, and Mohammed Bennamoun. Transformers in small object detection: A benchmark and survey of state-of-the-art. *ACM Computing Surveys*, 58(3):1–33, 2025.
- [23] Dilxat Muhtar, Zhenshi Li, Feng Gu, Xueliang Zhang, and Pengfeng Xiao. Lhrs-bot: Empowering remote sensing with vgi-enhanced large multimodal language model. In *European Conference on Computer Vision*, pages 440–457. Springer, 2024.
- [24] Shuo Ni, Di Wang, He Chen, Haonan Guo, Ning Zhang, and Jing Zhang. Unigeoseg: Towards unified open-world segmentation for geospatial scenes. *arXiv preprint arXiv:2511.23332*, 2025.
- [25] Alec Radford, Jong Wook Kim, Chris Hallacy, Aditya Ramesh, Gabriel Goh, Sandhini Agarwal, Girish Sastry, Amanda Askell, Pamela Mishkin, Jack Clark, et al. Learning transferable visual models from natural language supervision. In *International conference on machine learning*, pages 8748–8763. PMLR, 2021.
- [26] Nikhila Ravi, Valentin Gabeur, Yuan-Ting Hu, Ronghang Hu, Chaitanya Ryali, Tengyu Ma, Haitham Khedr, Roman Rädle, Chloe Rolland, Laura Gustafson, et al. Sam 2: Segment anything in images and videos. 2025:28085–28128, 2025.
- [27] Akashah Shabbir, Mohammed Zumri, Mohammed Bennamoun, Fahad Shahbaz Khan, and Salman Khan. Geopixel: Pixel grounding large multimodal model in remote sensing. In *International Conference on Machine Learning*, pages 54095–54111. PMLR, 2025.
- [28] Aaditya Singh, Adam Fry, Adam Perelman, Adam Tart, Adi Ganesh, Ahmed El-Kishky, Aidan McLaughlin, Aiden Low, AJ Ostrow, Akhila Ananthram, et al. Openai gpt-5 system card. *arXiv preprint arXiv:2601.03267*, 2025.
- [29] Xian Sun, Peijin Wang, Zhiyuan Yan, Feng Xu, Ruiping Wang, Wenhui Diao, Jin Chen, Jihao Li, Yingchao Feng, Tao Xu, et al. Fair1m: A benchmark dataset for fine-grained object recognition in high-resolution remote sensing imagery. *ISPRS Journal of Photogrammetry and Remote Sensing*, 184:116–130, 2022.
- [30] Yuxi Sun, Shanshan Feng, Xutao Li, Yunming Ye, Jian Kang, and Xu Huang. Visual grounding in remote sensing images. In *Proceedings of the 30th ACM International conference on Multimedia*, pages 404–412, 2022.
- [31] Fengxiang Wang, Mingshuo Chen, Xuming He, Yi-Fan Zhang, Yueying Li, Feng Liu, Zijie Guo, Zhenghao Hu, Jiong Wang, Jingyi Xu, et al. Omnearth-bench: Towards holistic evaluation of earth’s six spheres and cross-spheres interactions with multimodal observational earth data, 2025.

- [32] Fengxiang Wang, Hongzhen Wang, Zonghao Guo, Di Wang, Yulin Wang, Mingshuo Chen, Qiang Ma, Long Lan, Wenjing Yang, Jing Zhang, et al. Xlrs-bench: Could your multimodal llms understand extremely large ultra-high-resolution remote sensing imagery? In *Proceedings of the Computer Vision and Pattern Recognition Conference*, pages 14325–14336, 2025.
- [33] Fengxiang Wang, Mingshuo Chen, Yueying Li, Di Wang, Haotian Wang, Zonghao Guo, Zefan Wang, Shan Boqi, Long Lan, Yulin Wang, et al. Geollava-8k: scaling remote-sensing multimodal large language models to 8k resolution. *Advances in Neural Information Processing Systems*, 38:159185–159218, 2026.
- [34] Fengxiang Wang, Mingshuo Chen, Yueying Li, Yajie Yang, Yifan Zhang, Long Lan, Xue Yang, Hongda Sun, Yulin Wang, Di Wang, et al. Geoeyes: On-demand visual focusing for evidence-grounded understanding of ultra-high-resolution remote sensing imagery. *arXiv preprint arXiv:2602.14201*, 2026.
- [35] Jinwang Wang, Wen Yang, Haowen Guo, Ruixiang Zhang, and Gui-Song Xia. Tiny object detection in aerial images. In *2020 25th international conference on pattern recognition (ICPR)*, pages 3791–3798. IEEE, 2021.
- [36] Peng Wang, Shuai Bai, Sinan Tan, Shijie Wang, Zhihao Fan, Jinze Bai, Keqin Chen, Xuejing Liu, Jialin Wang, Wenbin Ge, et al. Qwen2-vl: Enhancing vision-language model’s perception of the world at any resolution. *arXiv preprint arXiv:2409.12191*, 2024.
- [37] Weiyun Wang, Zhangwei Gao, Lixin Gu, Hengjun Pu, Long Cui, Xingguang Wei, Zhaoyang Liu, Linglin Jing, Shenglong Ye, Jie Shao, et al. Internvl3. 5: Advancing open-source multimodal models in versatility, reasoning, and efficiency. *arXiv preprint arXiv:2508.18265*, 2025.
- [38] Gui-Song Xia, Xiang Bai, Jian Ding, Zhen Zhu, Serge Belongie, Jiebo Luo, Mihai Datcu, Marcello Pelillo, and Liangpei Zhang. Dota: A large-scale dataset for object detection in aerial images. In *Proceedings of the IEEE conference on computer vision and pattern recognition*, pages 3974–3983, 2018.
- [39] Dongjie Yang, Xianjun Gao, Yuanwei Yang, Kangliang Guo, Kuikui Han, and Lei Xu. Advances and future prospects in building extraction from high-resolution remote sensing images. *IEEE Journal of Selected Topics in Applied Earth Observations and Remote Sensing*, 18:6994–7016, 2025.
- [40] Licheng Yu, Patrick Poirson, Shan Yang, Alexander C Berg, and Tamara L Berg. Modeling context in referring expressions. In *European conference on computer vision*, pages 69–85. Springer, 2016.
- [41] Yang Zhan, Zhitong Xiong, and Yuan Yuan. Rsvg: Exploring data and models for visual grounding on remote sensing data. *IEEE transactions on geoscience and remote sensing*, 61:1–13, 2023.
- [42] Jingyi Zhang, Jiaying Huang, Sheng Jin, and Shijian Lu. Vision-language models for vision tasks: A survey. *IEEE transactions on pattern analysis and machine intelligence*, 46(8):5625–5644, 2024.
- [43] YiFan Zhang, Huanyu Zhang, Haochen Tian, Chaoyou Fu, Shuangqing Zhang, Junfei Wu, Feng Li, Kun Wang, Qingsong Wen, Zhang Zhang, et al. Mme-realworld: Could your multimodal llm challenge high-resolution real-world scenarios that are difficult for humans? 2025:89655–89701, 2025.
- [44] Ziwei Zheng, Michael Yang, Jack Hong, Chenxiao Zhao, Guohai Xu, Le Yang, Chao Shen, and Xing Yu. Deepeyes: Incentivizing "thinking with images" via reinforcement learning. *arXiv preprint arXiv:2505.14362*, 2025.
- [45] Kaiyang Zhou, Jingkang Yang, Chen Change Loy, and Ziwei Liu. Learning to prompt for vision-language models. *International journal of computer vision*, 130(9):2337–2348, 2022.

Appendix

Appendix Contents

Appendix A. Dataset Construction Details	13
A.1 Source Datasets and Image Filtering	13
A.2 Task Taxonomy and Instruction Schema	14
A.3 Split Construction and Data Statistics	15
Appendix B. Data Engine and Annotation Protocol	16
B.1 Programmatic Task Derivation	16
B.2 VLM-assisted Instruction Generation	17
B.3 Expert-led Annotation for Complex Tasks	18
B.4 Human Verification and Quality Control	19
Appendix C. Evaluation Protocol and Metrics	20
C.1 Output Format Normalization	20
C.2 Bounding Box Evaluation	21
C.3 Segmentation Evaluation	22
C.4 Counting and Option Evaluation	22
C.5 Overall Score Aggregation	23
Appendix D. MAP-Agent Implementation Details	23
D.1 Prompt Templates	23
D.2 ROI Discovery	23
D.3 Local Evidence Inspection	24
D.4 Global-Local Evidence Synthesis	25
D.5 Inference Cost and Hyperparameters	25
Appendix E. Additional Diagnostic and Robustness Analyses	26
E.1 Grounding Error Taxonomy	26
E.2 Error Diagnosis on Basic Grounding	27
E.3 Sensitivity to Scale	27
E.4 Coordinate Format Robustness	28
Appendix F. Qualitative Examples of UHR-Micro	29
Appendix G. Datasheets	30

A Dataset Construction Details

This section provides additional details on the construction of UHR-Micro, including source data selection, task schemas, and split construction.

A.1 Source Datasets and Image Filtering

DOTAv2. DOTAv2 [38] is a large-scale benchmark for object detection in aerial images, containing high-resolution scenes collected from diverse sensors and platforms. Its images exhibit substantial variations in object scale, orientation, density, and scene layout, making it well suited for constructing UHR tasks that require both global scene awareness and precise localization. DOTAv2 provides expert annotations in the form of arbitrary quadrilateral boxes over common aerial object categories, which allows us to derive coordinate-based grounding, detection, counting, and spatial-relation tasks. In UHR-Micro, we retain DOTAv2 images with 4K-scale long-edge resolution and sufficient target density and spatial diversity for deterministic micro-target evaluation.

FAIR1Mv2. FAIR1Mv2 [29] is designed for fine-grained object recognition in high-resolution remote sensing imagery. Compared with generic aerial detection datasets, FAIR1M provides richer category granularity, including fine-grained subcategories for objects such as aircraft, ships, vehicles,

Table 6: Source-wise image statistics of UHR-Micro after filtering. Average resolutions are rounded to the nearest hundred pixels.

Source Dataset	Images	Avg. Resolution	Avg. Pixels	Max. Resolution
DOTAv2 [38]	145	4800 × 4200	24.10 MP	29200 × 27620
FAIR1Mv2 [29]	77	5700 × 5800	34.42 MP	10000 × 9472
SODA-A [22]	863	4800 × 2800	13.26 MP	4762 × 4800
xView [12]	127	4300 × 3100	13.28 MP	4994 × 3187
Total	1212	4800 × 3200	15.90 MP	29200 × 27620

sports fields, and road-related targets. Its oriented bounding-box annotations and fine-grained labels are particularly useful for constructing tasks that require semantic discrimination among visually similar micro-targets, such as object classification and fine-grained recognition. We select UHR scenes from FAIR1Mv2 with 4K-scale long-edge resolution and reliable fine-grained annotations, enabling UHR-Micro to test whether VLMs can distinguish subtle target types under severe scale disparity.

SODA-A. SODA-A [22] is the aerial subset of the SODA benchmark, which was introduced to support large-scale small object detection. It focuses on aerial scenes with dense small objects and provides oriented box annotations across multiple object categories. This makes SODA-A especially relevant to UHR-Micro, where the central challenge is not merely object recognition but the discovery of extremely small task-relevant evidence within a large image canvas. We use SODA-A images to enrich micro-target density and to construct tasks involving dense enumeration, local discrimination, and crowded-scene grounding. Images are filtered to ensure UHR resolution, valid annotations, and deterministic target-answer correspondence.

xView. xView [12] is a large-scale overhead imagery dataset collected from WorldView-3 satellite imagery at 0.3m ground sample distance. It contains diverse geographic scenes and a broad taxonomy of object categories, with dense bounding-box annotations over small, rare, and fine-grained object types. The dataset is valuable for UHR-Micro because it introduces real-world satellite imagery with complex backgrounds, heterogeneous object distributions, and challenging small-object instances. We retain xView scenes that meet the UHR resolution criterion and contain sufficient annotated objects for constructing grounding, counting, and spatial reasoning instructions. All selected annotations are converted into the unified UHR-Micro schema before task generation.

Unified filtering and standardization. Across all source datasets, we apply a common filtering and standardization pipeline. We retain 4K-scale UHR images with valid spatial annotations and unambiguous target instances. Corrupted images, incomplete annotations, duplicated samples, and cases whose answers cannot be deterministically verified are removed. Source annotations are converted into a unified absolute-pixel annotation coordinate system and normalized into task-specific targets, including bounding boxes, polygonal masks, numerical answers, and discrete options. This filtering strategy ensures that UHR-Micro evaluates micro-level perception in native UHR scenes rather than artifacts of inconsistent annotation formats or ambiguous source labels.

Retained source statistics. Tab. 6 summarizes the source-wise composition and resolution statistics of UHR-Micro after filtering.

A.2 Task Taxonomy and Instruction Schema

UHR-Micro defines a unified instruction schema over 16 tasks, covering four complementary dimensions of micro-target perception: grounding, fine-grained understanding, counting, and spatial reasoning. Each instruction is paired with a deterministic target representation, allowing model responses to be parsed in a consistent and objective manner. Since remote sensing annotations naturally involve both horizontally aligned and oriented objects, UHR-Micro does not impose a single geometric convention across all localization tasks. Instead, the required answer representation is explicitly specified in each instruction.

Table 7: Instruction schema of UHR-Micro. The table summarizes the input condition and deterministic answer representation associated with each task. Evaluation protocols are described separately in Sec. C.

Dimension	Task	Input Condition	Answer Representation
Grounding	Global Detection (GD)	Full-image query	Multiple horizontal or oriented bounding boxes
	Regional Detection (RD)	Region-constrained query	Multiple horizontal or oriented bounding boxes
	Basic Grounding (BG)	Referring expression over the full image	Single horizontal or oriented bounding box
	Complex Grounding (CG)	Multi-hop spatial or relational expression	Single horizontal or oriented bounding box
	Multi-Condition Retrieval (MCR)	Multi-attribute and spatial-condition query	Multiple horizontal or oriented bounding boxes
Fine-grained Understanding	Object Classification (OC)	Indicated target in the full image	Multiple-choice option
	Fine-Grained Recognition (FGR)	Indicated target instance	Multiple-choice option
	Referring Segmentation (RS)	Referring expression over the full image	COCO-style compressed RLE mask
	Component Segmentation (CS)	Component-level expression	COCO-style compressed RLE mask
Counting	Global Counting (GC)	Full-image query	Integer answer
	Regional Counting (RC)	Region-constrained query	Integer answer
	Conditional Counting (CC)	Attribute- or region-conditioned query	Integer answer
	Cross-Region Compare (CRC)	Pair of regions or region descriptions	Integer answer
Spatial Reasoning	Directional Relationship (DrR)	Marked object pair	Multiple-choice option
	Distance Relationship (DsR)	Reference object and candidate objects	Multiple-choice option
	Pattern Distribution Recognition (PDR)	Full image with distribution options	Multiple-choice option

Geometric answer representations. For localization-oriented tasks, including *GD*, *RD*, *BG*, *CG*, and *MCR*, targets may be represented as either horizontal bounding boxes or oriented bounding boxes. A horizontal bounding box is encoded as $[x_1, y_1, x_2, y_2]$, while an oriented bounding box is encoded by four polygon vertices as $[x_1, y_1, x_2, y_2, x_3, y_3, x_4, y_4]$. Multi-target tasks require a sequence of such geometric primitives. In the released annotations, all target coordinates are stored as absolute pixel coordinates on the original image canvas. This design preserves the spatial precision required for UHR evaluation while remaining compatible with heterogeneous source annotations; model-facing prompts may use normalized coordinate conventions and are converted back to this absolute pixel space before scoring.

Region and visual-reference conventions. Region-conditioned tasks use heterogeneous but deterministic forms of spatial reference. In the annotation files, *RD* and *RC* primarily use rectangular regions stored in absolute pixel coordinates, which are converted to the model-facing coordinate protocol during benchmarking; *CRC* may involve either coordinate-defined regions or language-described regions. *CC* often uses natural-language regions of interest, such as a cleared strip, a storage zone, or a dense object cluster. For relational tasks, *DrR* and *DsR* identify reference objects and candidates through rendered visual markers, such as red, blue, or other colored boxes. *PDR* may operate on the full image, where the answer is selected from candidate distribution descriptions.

Segmentation representations. For both *RS* and *CS*, the released target is represented as a COCO-style compressed RLE mask, which can be decoded into a binary mask using the corresponding image size. *RS* focuses on object-level segmentation from referring expressions, whereas *CS* targets component-level segmentation from part descriptions.

A.3 Split Construction and Data Statistics

UHR-Micro is released with development, validation, and test partitions. The development partition provides diverse task instances for method exploration and prompt design. The validation partition is used for selecting inference-time configurations, such as crop size, region budget, and agentic reasoning strategies. The test partition is used for reporting final benchmark results. Unless otherwise specified, all results in the main paper are reported on the test partition. All main experiments are conducted without fine-tuning on the development or validation partitions.

Each instruction is paired with a deterministic target representation and evaluated under its corresponding task protocol. This design allows UHR-Micro to probe different perceptual skills, spatial regions, object instances, and reasoning conditions in UHR imagery while maintaining objective and reproducible evaluation.

As shown in Tab. 8, UHR-Micro contains 11,253 deterministic instructions across 16 tasks, including 4,832 development instructions, 1,600 validation instructions, and 4,821 test instructions. The validation partition is balanced across tasks with 100 instructions per task, supporting controlled configuration selection across the full taxonomy. The development and test partitions preserve broader task-specific distributions produced by the construction and filtering pipeline.

Table 8: Task-wise instruction statistics of UHR-Micro.

Task	Development	Validation	Test	Total
GD	670	100	569	1339
RD	276	100	296	672
BG	628	100	570	1298
CG	370	100	379	849
MCR	173	100	205	478
OC	676	100	583	1359
FGR	163	100	197	460
RS	115	100	149	364
CS	98	100	108	306
GC	296	100	304	700
RC	569	100	544	1213
CC	170	100	204	474
CRC	275	100	222	597
DrR	113	100	160	373
DsR	112	100	159	371
PDR	128	100	172	400
Total	4832	1600	4821	11253

B Data Engine and Annotation Protocol

This section expands the three-tier hybrid data engine introduced in the main paper. UHR-Micro is constructed to balance annotation scalability, semantic richness, and target determinism. Built upon dense ground-truth annotations from source remote sensing datasets, the pipeline combines programmatic derivation, VLM-assisted instruction generation, and expert-led annotation. The three tiers correspond to increasing levels of semantic and reasoning complexity: foundational tasks are generated from coordinates and categories through geometric rules; tasks requiring descriptive semantic alignment are assisted by frontier VLMs and cross-validated by human annotators; tasks involving deep spatial reasoning are led by domain experts with model assistance and rigorous review. Across all tiers, the final released instructions are restricted to deterministic answer formats, including bounding boxes, segmentation masks, exact numbers, and discrete options.

B.1 Programmatic Task Derivation

The first tier targets foundational perception tasks whose answers can be deterministically derived from dense source annotations. These tasks are primarily driven by coordinate mappings, category labels, instance geometries, object centers, and spatial relations. Representative examples include global detection, regional detection, object classification, fine-grained recognition, global or regional enumeration, and pairwise spatial-relation tasks. Programmatic derivation provides a scalable way to construct large numbers of evaluation instructions while preserving objective ground truth.

Localization and region-constrained tasks. For localization-oriented tasks, annotated object instances are grouped by image, category, and spatial scope. Global detection queries are constructed over the full native-resolution image, whereas regional detection queries restrict the search space to bounded sub-regions. Candidate regions are selected to contain valid target instances while avoiding ambiguous boundary cases or poorly supported regions. Depending on the source annotation and the instruction requirement, the expected answer may be represented as either horizontal bounding boxes or oriented bounding boxes. All generated annotation coordinates are retained in the original absolute-pixel image coordinate system to preserve the spatial precision required for UHR evaluation.

Category and fine-grained recognition. For category-level tasks, target instances are paired with category labels from source annotations. Object classification evaluates whether models can assign basic semantic categories to extremely small instances, while fine-grained recognition further requires distinguishing specific subtypes, such as aircraft or ship models. Multiple-choice options are constructed to include a unique correct answer and plausible distractors. When possible, distractors are sampled from semantically related or visually confusable categories, making the task focus on fine-grained recognition rather than trivial label elimination.

Global and regional enumeration. For numerical perception tasks with explicit spatial scopes, target counts are derived from verified annotation sets using deterministic enumeration rules. *Global Counting (GC)* requires exhaustive enumeration of all instances of a target category over the full image, while *Regional Counting (RC)* restricts enumeration to a bounded region. Candidate samples are checked to ensure that the queried category and spatial scope lead to a well-defined integer answer. These tasks provide foundational tests of dense micro-target enumeration under native UHR resolution.

Spatial relationship reasoning. Spatial-relation tasks are generated from annotated object locations and geometric configurations. Directional relationship tasks evaluate relative orientation between marked objects, while distance relationship tasks compare distances from a reference object to multiple candidates. Candidate pairs or sets are filtered to avoid visually ambiguous cases, such as nearly identical distances or unstable directional assignments. This produces deterministic spatial-reasoning questions while retaining the micro-target scale and cluttered context of UHR scenes.

B.2 VLM-assisted Instruction Generation

The second tier addresses tasks that require descriptive semantic alignment beyond direct coordinate or category mapping. In these cases, frontier VLMs are used to assist the generation of natural-language descriptions, referring expressions, distribution descriptions, and candidate options. Importantly, the VLMs are not used as the sole source of ground truth. The final targets remain anchored in source annotations or curated target sets, while generated language is cross-validated by human annotators to ensure semantic correctness, target uniqueness, and consistency with the visual evidence.

Basic grounding. Basic grounding requires a model to identify a unique target from a natural-language referring expression. To construct such samples, candidate target instances are first selected from annotated objects. A VLM is then used to generate referring expressions based on visible spatial, contextual, or appearance cues. Human annotators cross-validate the generated descriptions to ensure that the expression uniquely refers to the intended target and does not accidentally match nearby or visually similar distractors. Ambiguous, under-specified, or visually unsupported descriptions are revised or removed.

Pattern distribution recognition. Pattern distribution recognition evaluates whether models can understand the global arrangement of object groups. For this task, object locations and distribution layouts are first derived from annotations. A VLM-assisted process is then used to formulate distribution-level descriptions and plausible distractor options. Human validation focuses on whether the correct option accurately describes the observed spatial pattern and whether the distractors remain plausible but clearly incorrect. This construction allows UHR-Micro to test topological and distributional perception rather than only local object recognition.

Language quality and semantic alignment. For all VLM-assisted samples, generated instructions are checked for grammatical validity, semantic faithfulness, and absence of answer leakage. Descriptions that rely on vague visual cues, ambiguous spatial references, or unstable contextual assumptions are revised or filtered. This tier therefore combines the linguistic diversity of VLM generation with human control over the final semantic alignment between instruction and visual target.

Representative prompt design. Tabs. 9–11 summarize the representative prompt families used in VLM-assisted dataset construction. These prompts restrict VLMs to region describability assessment, language generation, structured question writing, or hard-negative selection. The VLM is not used as the sole source of ground truth: final geometric targets, counts, categories, and masks remain determined by source annotations, curated candidate sets, or rule-based geometry. The structured outputs enable automatic parsing, consistency checking, rejection, and human review. Across these prompt families, VLM outputs are treated as candidate language annotations or option-generation aids rather than final ground truth. The final answers are determined by source annotations, curated object sets, or deterministic geometric rules, and all language-heavy samples are checked through automatic validation and human review.

Table 9: Representative prompts for region-level reference construction. These prompts support region-constrained tasks by producing concise and uniquely identifiable region descriptions.

Prompt family	Used for	Core objective	Validation role
Region descriptability assessment	RD / region references	Judge whether a visualized candidate region is functionally coherent, spatially complete, and uniquely describable by a concise natural-language phrase. The prompt discourages vague references and asks for minimal disambiguation when similar regions exist.	Selects or refines natural region references; low-confidence or ambiguous regions are filtered or revised.
Region-level reference generation	CG / CRC support	Generate a short description for a highlighted region using visible cues such as relative position, shape, adjacency, roads, water, buildings, coastline, or land-use pattern. The prompt forbids mentioning boxes, polygons, metadata, counts, or annotation hints.	Provides natural region context for complex reasoning tasks while reducing answer leakage from annotations.

B.3 Expert-led Annotation for Complex Tasks

The third tier targets tasks requiring deep reasoning, multi-condition constraints, complex numerical comparison, or region-level semantic interpretation. These tasks are led by domain experts with model assistance. Source annotations provide the geometric foundation, while experts construct, inspect, and refine the reasoning conditions to ensure that each instruction has a unique and visually grounded answer. This tier is particularly important for complex grounding, multi-condition retrieval, conditional counting, cross-region comparison, and mask-level understanding, where simple templates are insufficient to capture the intended reasoning structure.

Complex grounding. Complex grounding requires multi-step or multi-hop reasoning over spatial and relational cues. Experts construct or refine instructions that identify a target through ordinal positions, dense clusters, neighboring objects, region-level layouts, or combinations of multiple spatial relations. Model assistance may be used to propose candidate descriptions or summarize local structures, but the final instruction is reviewed to ensure that it points to one unambiguous target. Samples are revised or discarded when the description is visually weak, under-specified, or compatible with multiple valid targets.

Multi-condition retrieval. Multi-condition retrieval extends grounding from single-object localization to set-level retrieval. Each instruction combines multiple constraints, such as category, region, appearance, contextual relation, spatial arrangement, or exclusion conditions. The answer consists of all targets satisfying the full condition set. Expert review focuses on answer-set completeness, condition clarity, and the removal of cases where the textual constraints are too broad, too narrow, or visually ambiguous.

Conditional counting and cross-region comparison. Conditional counting and cross-region comparison are treated as expert-led numerical reasoning tasks because their correctness depends not only on object enumeration, but also on semantic constraint interpretation, region validity, and answer determinism. For *Conditional Counting (CC)*, experts inspect or refine the counting condition to ensure that the target set is clearly defined by the specified category, visual attribute, contextual cue, or region description. For *Cross-Region Compare (CRC)*, experts verify the two regions, the target populations within each region, and the comparison semantics before assigning the final numerical answer. Samples with ambiguous region boundaries, unstable object membership, unclear semantic constraints, or unreliable comparisons are revised or removed. This process ensures that complex

Table 10: Representative prompts for grounding-oriented instruction generation and verification. These prompts support unique target reference, distractor checking, and complex grounding question construction.

Prompt family	Used for	Core objective	Validation role
Basic referring-expression generation	BG	Generate one natural referring expression for a target instance using the image, same-category distractors, and numeric layout. The prompt forbids mentioning annotations, colors, coordinates, indices, or box markers.	Ensures that the expression uniquely contrasts the target against same-category distractors using visible spatial or contextual cues.
Referring-expression verification	BG quality control	Review whether the generated expression is unambiguous and consistent with the full geometric layout, especially ordinal or directional claims.	Detects ambiguous references, contradictory spatial phrases, and expressions that could match multiple instances.
Cross-instance audit	BG quality control	Re-render same-category distractors as candidate targets and test whether the original referring expression incorrectly fits them.	Identifies cross-instance misidentification; failed samples are revised or removed.
Complex grounding question generation	CG	Given a region reference, candidate targets, local structures, ordered member lists, scene profiles, and visual-anchor hints, select one target and write a hard but unambiguous question requiring multi-step spatial or relational reasoning.	Checks target ID, structure ID, rank, and question consistency; ambiguous or weak questions are revised or filtered.

counting tasks evaluate controlled numerical reasoning over localized micro-evidence rather than artifacts of underspecified textual queries.

Mask-level annotation. For referring segmentation and component segmentation, UHR-Micro provides mask-level targets in COCO-style compressed RLE format. Referring segmentation focuses on object-level masks specified by textual descriptions, while component segmentation targets visually identifiable object parts, such as aircraft empennages or other fine structures. These samples undergo additional inspection to ensure that the mask corresponds to the intended object or component and that the target is visually meaningful at UHR scale.

B.4 Human Verification and Quality Control

All instructions are subjected to manual verification or rule-based consistency checks before inclusion. The quality-control process is designed to ensure that each sample has a deterministic target, follows the required output format, and avoids subjective interpretation. Task-specific automatic checks cover format validity, coordinate consistency, duplicate removal, option uniqueness, and numerical consistency, while human annotators focus on semantic correctness, ambiguity removal, and visual grounding for language-heavy or reasoning-intensive samples.

Format validation. Localization answers are checked for valid bounding-box formats and consistency with the required horizontal or oriented representation. Segmentation answers are checked for valid COCO-style compressed RLE encoding and compatibility with the corresponding image size. Counting answers are verified as exact integer values, and multiple-choice tasks are checked to ensure that the correct option is unique.

Table 11: Representative prompts for pattern distribution recognition. These prompts generate coarse distribution descriptions and hard negative options without using the VLM as the source of final ground truth.

Prompt family	Used for	Core objective	Validation role
Distribution description generation	PDR	Given a highlighted image and target-center coordinates, generate a coarse spatial distribution description. The prompt requires high-level layout language and forbids category names, exact counts, coordinate copying, and boilerplate phrasing.	Produces the correct distribution option while controlling category leakage and overly detailed enumeration.
Distribution hard-negative selection	PDR	Given a gold distribution description and candidate descriptions from other images, select descriptions whose spatial meanings are most different from the reference.	Constructs plausible but incorrect multiple-choice options; invalid selections are rejected or replaced by heuristic fallback.

Geometric and numerical consistency. For region-based tasks, candidate regions are checked for valid extent, target inclusion, and boundary ambiguity. Spatial-relation tasks are filtered to ensure that directional or distance-based answers are visually distinguishable from distractors. Counting and comparison tasks are verified against annotated target sets and manually inspected when semantic constraints or region definitions introduce ambiguity.

Semantic and ambiguity checks. For language-heavy tasks, human annotators inspect whether the instruction faithfully describes the intended target or target set. Referring expressions are checked against nearby distractors, complex grounding descriptions are checked for uniqueness, and multi-condition retrieval queries are checked for answer-set completeness. Conditional counting and cross-region comparison samples are further reviewed for semantic clarity, region validity, and deterministic numerical answers.

Final filtering. After task-specific validation and manual review where needed, samples with unresolved ambiguity, invalid target formats, inconsistent annotations, duplicate answers, or unverifiable visual evidence are removed. This process preserves the scalability of automatic generation while maintaining the reliability required for objective evaluation of micro-level perception in UHR imagery.

C Evaluation Protocol and Metrics

This section defines the deterministic evaluation protocol used in UHR-Micro. The benchmark contains heterogeneous answer formats, including bounding boxes, segmentation masks, exact numerical values, and discrete options. A single metric cannot faithfully evaluate all these formats. We therefore use format-specific metrics, normalize all scores to $[0, 1]$, and multiply them by 100 for reporting. Empty, invalid, or unparseable predictions are assigned a score of zero. This protocol ensures that different task families remain comparable while preserving the semantics of their expected outputs.

C.1 Output Format Normalization

Before scoring, model outputs are normalized into canonical answer formats according to the instruction associated with each sample. This step is necessary because VLMs often produce free-form text, explanations, or partially structured answers even when prompted to output deterministic formats. The parser first removes irrelevant surrounding text when possible and then attempts to extract the required answer type.

Bounding-box outputs. For localization tasks, the required geometric representation is specified in the instruction. A horizontal bounding box is parsed as $[x_1, y_1, x_2, y_2]$, where (x_1, y_1) and (x_2, y_2) denote the top-left and bottom-right corners. An oriented bounding box is parsed as four polygon vertices, $[x_1, y_1, x_2, y_2, x_3, y_3, x_4, y_4]$.

For multi-target tasks, the parser extracts a list of such boxes. The coordinate values are interpreted according to the model-facing protocol used in the prompt. All parsed boxes are then converted to absolute pixel coordinates on the original image canvas before scoring. Predictions are considered invalid if they contain non-numeric coordinates, have an incorrect number of coordinates, use the wrong geometric format, produce degenerate boxes, or cannot be mapped to the requested representation.

Segmentation outputs. For segmentation tasks, VLM predictions are parsed as box prompts under the corresponding coordinate protocol and converted to absolute pixel coordinates before being passed to SAM2. The resulting masks are encoded as COCO-style compressed RLE masks for evaluation. Invalid boxes, failed SAM2 masks, masks with incompatible dimensions, or empty masks are assigned zero.

Counting outputs. For counting tasks, the parser extracts a single integer from the model response. Responses containing multiple conflicting numbers are treated as invalid unless one number can be unambiguously identified as the final answer. Negative counts and non-integer answers are invalid. This normalization ensures that counting tasks evaluate numerical perception rather than natural-language explanation quality.

Discrete-option outputs. For multiple-choice tasks, model outputs are normalized to canonical option labels, such as A, B, C, and D. We allow common variants such as “Option A”, “A.”, or “The answer is A” to map to the same label. If the output contains no valid option label or contains multiple conflicting options, it is treated as incorrect.

C.2 Bounding Box Evaluation

Bounding-box evaluation is used for localization-oriented tasks, including detection, grounding, and multi-condition retrieval. These tasks require models to identify where micro-targets are located in a native UHR image. A hard IoU threshold is often brittle for this setting: because micro-targets occupy only a tiny fraction of the image, a small coordinate shift can cause a large IoU drop even when the prediction is visually close to the target. Conversely, a metric based only on center distance ignores object extent. We therefore use a continuous localization score that combines overlap and center proximity.

Single-target box scoring. Let g denote the ground-truth box and p the predicted box. Both horizontal and oriented boxes are converted to polygonal regions for overlap computation. Let $\text{IoU}(g, p)$ be their intersection-over-union. Let $d(g, p)$ be the Euclidean distance between the centers of g and p , and let σ_g be the diagonal length of the minimum enclosing horizontal box of the ground-truth target. The single-box score is defined as:

$$S_{\text{box}}(g, p) = \text{IoU}(g, p) + (1 - \text{IoU}(g, p)) \exp\left(-\frac{d(g, p)^2}{\sigma_g^2}\right).$$

The score is bounded in $[0, 1]$. A perfect prediction receives a score of 1. Predictions with high overlap receive high scores, while predictions with low overlap may still receive partial credit if they are close to the target center. This design is intended to reduce excessive brittleness for micro-scale targets while still rewarding precise localization.

Single-target grounding tasks. For single-target grounding tasks, such as basic grounding and complex grounding, the parsed prediction is matched directly to the unique ground-truth target. If the output is invalid or contains no valid box, the score is zero. If multiple boxes are returned for a single-target task, we use the highest-scoring valid box as the model’s predicted localization and treat the remaining boxes as extraneous outputs during parsing. This prevents a model from being rewarded for verbose outputs while still allowing robust evaluation of partially structured responses.

Multi-target detection and retrieval. For multi-target tasks, such as global detection, regional detection, and multi-condition retrieval, the prediction is a set of boxes and the ground truth is also a set of boxes. We perform one-to-one matching between predicted and ground-truth boxes using greedy matching based on S_{box} . At each step, the unmatched predicted–ground-truth pair with the highest score is selected, and both boxes are removed from further matching. This continues until no valid pairs remain.

Let T be the sum of the matched box scores. Let P_{fp} be the number of unmatched predicted boxes, and let N_{fn} be the number of unmatched ground-truth boxes. We define soft precision and soft recall as:

$$P_{\text{soft}} = \frac{T}{T + P_{\text{fp}}}, \quad R_{\text{soft}} = \frac{T}{T + N_{\text{fn}}}.$$

The final set-level localization score is the soft F-score:

$$F_{\text{soft}} = \frac{2P_{\text{soft}}R_{\text{soft}}}{P_{\text{soft}} + R_{\text{soft}}}.$$

If the denominator is zero, the score is set to zero. This set-based score jointly captures target coverage, spatial accuracy, false positives, and missed objects. It is better suited to free-form VLM outputs than confidence-ranked detection metrics such as AP, because most VLMs do not naturally produce calibrated confidence scores or ranked detection lists.

C.3 Segmentation Evaluation

Segmentation tasks are evaluated against mask-level targets. Under our VLM benchmarking protocol, models output boxes that are converted into SAM2-generated masks, and we evaluate these masks using a continuous mask score that mirrors the box localization metric while replacing box overlap with mask overlap. This is useful for UHR-Micro because component-level targets may be extremely small, and a hard mask-IoU threshold can be overly brittle for slight spatial shifts.

Let m denote the ground-truth mask and \hat{m} the predicted mask. Let $\text{IoU}_{\text{mask}}(m, \hat{m})$ be the mask intersection-over-union. Let $d(m, \hat{m})$ be the Euclidean distance between the foreground centroids of the two masks, and let σ_m be the diagonal length of the bounding box enclosing the ground-truth mask. The mask score is:

$$S_{\text{mask}}(m, \hat{m}) = \text{IoU}_{\text{mask}}(m, \hat{m}) + (1 - \text{IoU}_{\text{mask}}(m, \hat{m})) \exp\left(-\frac{d(m, \hat{m})^2}{\sigma_m^2}\right).$$

This score is also bounded in $[0, 1]$. It gives full credit to exact mask alignment, partial credit to predictions that are spatially close to the target, and low credit to predictions that are both non-overlapping and far from the target. Invalid, empty, or undecodable masks receive zero. If a task expects a single mask but the model returns multiple masks, we evaluate the best valid mask against the ground truth and ignore invalid masks.

C.4 Counting and Option Evaluation

Counting and discrete-option tasks use non-geometric answer formats. Their metrics are designed to match the semantics of the expected output while remaining robust to free-form VLM responses.

Counting score. For counting tasks, let c and \hat{c} denote the ground-truth and predicted counts, respectively. Although the required output is an exact integer, exact-match accuracy can be overly harsh when the true count is large. For example, predicting 49 instead of 50 reflects a much smaller error than predicting 1 instead of 2, even though both are off by one. We therefore use a bounded relative counting score:

$$M_{\text{cnt}}(c, \hat{c}) = \begin{cases} \max\left(0, 1 - \frac{|\hat{c}-c|}{c}\right), & c > 0, \\ \mathbf{1}[\hat{c} = 0], & c = 0. \end{cases}$$

This metric assigns full credit to exact counts and decreases linearly with relative error. Predictions with relative error greater than or equal to 100% receive zero. When the ground-truth count is zero, only a predicted count of zero receives credit. Unparsable or invalid numerical outputs are assigned zero.

Discrete-option accuracy. For multiple-choice tasks, including object classification, fine-grained recognition, directional relationship, distance relationship, and pattern distribution recognition, we use exact option accuracy. A prediction receives a score of 1 if its normalized option label matches the ground-truth option, and 0 otherwise:

$$M_{\text{opt}}(y, \hat{y}) = \mathbf{1}[\hat{y} = y].$$

Exact accuracy is appropriate for these tasks because the answer space is closed and all valid options are explicitly provided in the instruction. This avoids ambiguity in evaluating natural-language category names or relation descriptions.

C.5 Overall Score Aggregation

All sample-level scores are normalized to $[0, 1]$ using the metric corresponding to their answer format. For each task t , we compute the task score S_t as the average score over all samples in that task:

$$S_t = \frac{1}{N_t} \sum_{i=1}^{N_t} s_{t,i},$$

where N_t is the number of evaluated samples for task t and $s_{t,i}$ is the normalized score of the i -th sample.

The overall UHR-Micro score is computed as the macro-average over all 16 task scores:

$$S_{\text{overall}} = \frac{1}{16} \sum_{t=1}^{16} S_t.$$

Dimension-level scores are computed by averaging the task scores within each dimension. For example, the grounding score is the average over *GD*, *RD*, *BG*, *CG*, and *MCR*, while the counting score is the average over *GC*, *RC*, *CC*, and *CRC*. We use macro-averaging rather than sample-level micro-averaging to prevent high-volume tasks from dominating the final result. This ensures that each perceptual capability in the UHR-Micro taxonomy contributes equally to the benchmark score.

Unless otherwise specified, all tables report scores after multiplying the normalized values by 100. Thus, a reported score of 45.0 corresponds to a normalized score of 0.45.

D MAP-Agent Implementation Details

This section provides implementation details for reproducing MAP-Agent. MAP-Agent is a training-free inference framework that turns UHR perception into an explicit global-to-local evidence acquisition process. Instead of asking a VLM to answer directly from the entire UHR image, MAP-Agent decomposes inference into three stages: query-guided ROI discovery, localized evidence inspection, and global-local evidence synthesis. This design allows the model to first identify where task-relevant evidence may exist, then inspect native-resolution crops, and finally aggregate localized observations into a task-specific final answer.

D.1 Prompt Templates

The prompt templates are format-conditioned: for localization tasks, the required geometric representation is inherited from the original instruction, which may request either a horizontal bounding box or an oriented bounding box. Segmentation tasks are handled separately by predicting a horizontal box prompt for SAM2-based mask generation. MAP-Agent uses structured zero-shot prompts for each inference stage. The prompts are designed to enforce role separation across stages: the first stage proposes candidate regions without solving the task, the second stage inspects local visual evidence within ROI crops, and the third stage synthesizes local observations into the final answer. Representative prompt templates are summarized in Tabs. 12–14. The full prompt set will be released with the benchmark code.

D.2 ROI Discovery

The first stage performs query-guided ROI discovery over the full UHR image. The backbone VLM receives the full image and the task query, but it is not asked to solve the task directly. Instead, it

Table 12: Representative prompt template for query-guided ROI discovery.

ROI Discovery Prompt
<p>You are viewing the full ultra-high-resolution remote sensing image. The image size is given by its height and width. Under the default benchmarking protocol, all coordinates should be expressed in a full-image 1000-base coordinate system, where $x = 0$ is the left edge, $x = 1000$ is the right edge, $y = 0$ is the top edge, and $y = 1000$ is the bottom edge. Given the task query, identify candidate regions that are most likely to contain task-relevant visual evidence. Return only representative point coordinates for these regions. Do not provide the final answer, do not output bounding boxes, masks, counts, or option letters, and do not include explanations. The output should be a JSON-like list of points, e.g., $[[x_1, y_1], [x_2, y_2], \dots]$.</p>

Table 13: Representative prompt template for localized evidence inspection.

Local Evidence Inspection Prompt
<p>You are viewing one 1024×1024 ROI crop from a larger remote sensing image. Answer only using visual evidence inside this ROI. Under the default benchmarking protocol, all coordinates, if required, should use the ROI-local 1000-base coordinate system, where $x = 0$ is the left edge of the crop, $x = 1000$ is the right edge, $y = 0$ is the top edge, and $y = 1000$ is the bottom edge. Do not use full-image coordinates. For localization tasks, follow the geometric output format required by the instruction: use $[x_1, y_1, x_2, y_2]$ for a horizontal bounding box, or $[x_1, y_1, x_2, y_2, x_3, y_3, x_4, y_4]$ for an oriented bounding box. For multi-target tasks, output a list of boxes in the required format. If the target is not visible in this ROI, output <code>null</code>. For counting tasks, output one Arabic numeral. For multiple-choice tasks, output only the option letter. For segmentation tasks, output a tight horizontal bounding box to be used as a downstream SAM2 box prompt.</p>

predicts representative points that are likely to correspond to task-relevant evidence. Under the default benchmarking protocol, these points are expressed in a full-image 1000-base coordinate system. This normalized coordinate convention makes the prompt independent of the native image resolution while still allowing deterministic conversion back to absolute pixel coordinates.

Predicted points are converted into square ROI windows on the original image. Unless otherwise specified, MAP-Agent uses a crop side length of $S = 1024$ pixels. When a proposed ROI extends beyond the image boundary, its coordinates are clipped to the valid image extent; if the resulting crop is smaller than 1024×1024 , it is padded to the standard crop size. Overlapping candidate regions are suppressed to avoid redundant local inspection. If the query already specifies an explicit region, MAP-Agent can use the provided spatial constraint to construct the corresponding ROI directly.

MAP-Agent uses task-adaptive ROI allocation. Global search and multi-target retrieval tasks are assigned a larger ROI budget because relevant evidence may be distributed across the image. Segmentation tasks use two candidate ROIs by default to improve the chance of capturing the referred object or component. More localized tasks use a smaller default budget, reflecting their narrower evidence requirements. This allocation strategy balances evidence coverage and inference cost.

D.3 Local Evidence Inspection

The second stage performs localized evidence inspection on each selected ROI crop. Each crop is processed independently by the same backbone VLM. The model receives the ROI crop and an ROI-local version of the original task query, and is instructed to answer only based on visible evidence inside the crop. This restriction is important: it prevents the local stage from relying on unsupported global priors and forces the model to verify whether the queried evidence is actually present in the crop.

For localization-oriented tasks under the default benchmarking protocol, the local model outputs a bounding box in the ROI-local 1000-base coordinate system or `null` if the target is not visible. For multi-target tasks, it may output multiple local boxes. For counting tasks, it outputs a local count. For multiple-choice tasks, it outputs an option letter when the crop provides sufficient evidence. For

Table 14: Representative prompt template for global-local evidence synthesis.

Global-Local Evidence Synthesis Prompt

You are viewing the original full image together with selected ROI regions. The ROI-local observations have already been mapped to the full-image 1000-base coordinate system under the default benchmarking protocol. Use the original question and the localized evidence to produce the final answer in the required task-specific format. For localization tasks, preserve the geometric format requested by the instruction: horizontal bounding boxes should be returned as $[x_1, y_1, x_2, y_2]$, while oriented bounding boxes should be returned as $[x_1, y_1, x_2, y_2, x_3, y_3, x_4, y_4]$. For multi-target tasks, aggregate consistent boxes from multiple ROIs and remove duplicates when necessary. For counting and multiple-choice tasks, return the required integer or option letter. For segmentation tasks, return a single horizontal bounding box for SAM2-based mask generation. Avoid inventing objects or regions that are not supported by localized observations. The final response must end with a line beginning with `Final answer :`.

segmentation tasks, the local model also outputs a bounding box rather than a mask; the box is later used as a prompt for SAM2 to generate the segmentation mask.

All local coordinate outputs are first mapped back to the full-image 1000-base coordinate system using the ROI offset and crop size, and later converted to absolute pixel coordinates for evaluation. This produces a set of spatially grounded local observations, each associated with the ROI from which it was obtained. These mapped observations are then passed to the final synthesis stage.

D.4 Global-Local Evidence Synthesis

The third stage aggregates localized observations into the final answer. MAP-Agent provides the backbone VLM with the original question, the selected ROI evidence, and an image view in which selected ROIs are visually indicated. For geometric tasks, local predictions are first mapped from ROI-local coordinates to the full-image coordinate convention used by the current benchmarking protocol. The synthesis prompt then asks the model to select, aggregate, or deduplicate candidate outputs according to the required task format.

For single-target grounding tasks, the synthesis stage selects the most plausible localized candidate. For multi-target detection and retrieval tasks, it aggregates candidate boxes from multiple ROIs and removes duplicates. For counting tasks, it combines local numerical evidence according to the task query. For multiple-choice tasks, it uses ROI evidence to select the final option. This stage is designed to ground the final answer in localized observations rather than relying solely on a global-image guess.

For segmentation tasks, the final synthesized output is a bounding box for the referred object or component. The predicted box is converted to absolute pixel coordinates and used as a box prompt for SAM2. SAM2 then generates the final mask, which is stored in COCO-style compressed RLE format. If the final box is invalid or cannot be parsed, the segmentation prediction is treated as invalid and receives zero under the evaluation protocol.

D.5 Inference Cost and Hyperparameters

MAP-Agent uses the same backbone VLM as the corresponding baseline model. In the main experiments, the default crop size is $S = 1024$. Coordinates in prompts are represented using a 1000-base coordinate system by default, while models or APIs with a defined native coordinate convention are evaluated under their native convention when applicable. In all cases, final parsed outputs are converted back to absolute pixel coordinates for evaluation. The default decoding configuration uses deterministic generation with temperature 0.0 and top- p equal to 1.0.

The number of VLM calls per query depends on the number of selected ROIs. In general, MAP-Agent requires one full-image call for ROI discovery when needed, one local inspection call per ROI, and one final synthesis call. Thus, the inference cost can be summarized as

$$N_{\text{calls}} = \mathbf{1}_{\text{ROI}} + K + 1,$$

where K is the number of inspected ROI crops and $\mathbf{1}_{\text{ROI}}$ indicates whether the query requires model-based ROI discovery. SAM2 calls for segmentation are not counted as VLM calls.

Under the default task-adaptive ROI allocation, the validation-set implementation averages approximately 3.53 full-pipeline VLM calls per query. This cost is substantially lower than exhaustive sliding-window traversal while still allowing MAP-Agent to inspect native-resolution local evidence. The key advantage of MAP-Agent is therefore not simply using more image crops, but allocating visual inspection to query-relevant regions and aggregating the resulting micro-evidence into a final answer.

E Additional Diagnostic and Robustness Analyses

This section provides additional analyses beyond the main benchmark tables. The main paper reports a post-hoc error diagnosis on *Complex Grounding (CG)*, where MAP-Agent improves the success rate from 6.9% to 16.8% over the Qwen3-VL-8B baseline. Here, we first formalize the diagnostic taxonomy used for grounding tasks, then provide an additional diagnosis on *Basic Grounding (BG)*. We further analyze grounding performance with respect to target category, target scale, and local crowding, and finally examine the robustness of representative VLMs to different coordinate conventions.

E.1 Grounding Error Taxonomy

For grounding diagnostics, each prediction is assigned to one mutually exclusive category according to a fixed priority order. The diagnostic labels are assigned by rule-based checks where possible and manually verified for ambiguous cases. The taxonomy is designed to separate failures caused by invalid outputs, incorrect region selection, object hallucination, category confusion, contextual mismatch, and imprecise localization.

Invalid format (IF). The model output does not follow the required localization format or cannot be parsed into a valid box. This includes missing coordinates, non-numeric outputs, malformed boxes, empty responses, or answers that provide explanations instead of the requested localization result.

Region hallucination (RH). The prediction falls outside the annotated semantic region or the spatial scope required by the instruction. This category is mainly used for complex grounding tasks where the query specifies a region, layout, or contextual area before identifying the target. RH indicates a failure in global-to-local region selection.

Object hallucination (OH). The prediction does not overlap any valid annotated object and instead localizes background patterns, roads, shadows, buildings, or other non-target regions. This error indicates that the model produces a plausible-looking location without grounding it in actual object evidence.

Category hallucination (CatH). The prediction overlaps a valid annotated object, but the object category does not match the queried target category. This error indicates that the model identifies an object-like region but confuses its semantic class.

Context hallucination (CtxH). The prediction localizes an object of the correct category but fails to satisfy the referring condition or contextual constraint. For example, the model may select another instance of the same category that is located in the wrong spatial context, ordinal position, cluster, or relation.

Coordinate shift (CS). The prediction corresponds to the intended target but is not sufficiently accurate in coordinates. This includes shifted, enlarged, or poorly aligned boxes around the correct object. Coordinate shift reflects the difficulty of precise micro-target localization even when the model has roughly found the correct evidence.

Other failures (Oth.). This category includes rare or ambiguous errors that cannot be reliably assigned to the above categories.

Table 15: Error diagnosis on *Basic Grounding (BG)*. Each entry reports count and percentage. IFE, OH, CatH, CtxH, CS, Oth., and Succ. denote instruction-following error, object hallucination, category hallucination, context hallucination, coordinate shift, other failures, and successful localization, respectively.

Model	OH	CatH	CtxH	CS	IFE	Oth.	Succ.
GPT-5.2	91.2%	2.9%	0.4%	2.5%	0.4%	1.6%	1.1%
Qwen3-VL-8B	32.5%	19.2%	6.5%	12.6%	5.8%	2.5%	21.0%
MAP-Agent	31.8%	20.3%	6.5%	9.3%	1.4%	2.3%	28.4%

Success (Succ.). A prediction is counted as successful when it satisfies the grounding success criterion. In the main CG diagnosis, predictions with IoU ≥ 0.3 to the ground-truth target are counted as successful cases.

E.2 Error Diagnosis on Basic Grounding

The main paper reports diagnostic results on *CG*, where region hallucination remains the dominant residual error after applying MAP-Agent. To complement this analysis, we further diagnose *BG*, which removes much of the complex region-level reasoning required by *CG* and focuses on simpler target grounding. Since *BG* does not rely on the same semantic-region structure as *CG*, we use the same taxonomy except for region hallucination.

Tab. 15 shows the *BG* diagnostic results. GPT-5.2 is dominated by object hallucination, with 91.2% of its predictions falling on background or non-target regions. This indicates that its primary failure mode in native UHR scenes is not fine-grained recognition after localization, but the inability to reliably locate task-relevant micro-evidence in a large image canvas. This observation is consistent with Tab. 2: GPT-5.2 achieves much stronger *BG* performance when the target is provided in localized Oracle GT-Crop settings, reaching 48.8 under 512-pixel crops and 29.1 under 1024-pixel crops, but its performance drops sharply to 12.3 under 2048-pixel crops and only 3.9 under native full-image input. The high object-hallucination rate therefore suggests that, as the visual context expands and the target occupies a smaller relative area, GPT-5.2 frequently fails to identify the correct region and instead grounds its answer on spurious background patterns.

By contrast, Qwen3-VL-8B shows stronger native UHR grounding behavior. Its object-hallucination rate is reduced to 32.5%, and its *BG* success rate reaches 21.0%, substantially higher than GPT-5.2 under the same native setting. Although Qwen3-VL-8B still suffers from category hallucination and context hallucination, it more often reaches real object evidence before making a semantic or contextual mistake. This stronger large-canvas localization ability is one of the reasons we select Qwen3-VL-8B as a primary backbone for MAP-Agent.

MAP-Agent further improves the success rate from 21.0% to 28.4% over the Qwen3-VL-8B baseline. The gain is accompanied by fewer instruction-following errors and reduced coordinate shift, indicating that localized evidence inspection stabilizes both answer formatting and final localization. Object hallucination remains the largest residual error, showing that reliable discovery of task-relevant micro-evidence remains challenging even for basic referring expressions.

Taken together with the *CG* diagnosis in the main paper, the *BG* results reveal two complementary failure modes. GPT-5.2 primarily fails at discovering valid object evidence in native large-canvas settings, whereas Qwen3-VL-8B more often reaches real objects but still confuses category or context. In *CG*, once complex spatial or relational constraints are introduced, the bottleneck further shifts toward region selection and context-consistent target identification. These findings support the central motivation of MAP-Agent: UHR reasoning requires not only recognizing micro-targets, but also actively finding and verifying localized evidence under task-specific constraints.

E.3 Sensitivity to Scale

We analyze how grounding performance varies with target scale on *Basic Grounding (BG)* and *Complex Grounding (CG)*. Both tasks require single-target localization and can be directly aligned with object-level annotations, making them suitable for studying the relationship between target size and localization reliability. Target size is measured by the target side length, and localization

Table 16: Correlation between target size and localization performance on *Basic Grounding (BG)* and *Complex Grounding (CG)*. Target size is measured by the target side length. Pearson correlation measures linear association, while Spearman correlation measures rank-level monotonic association.

Model	Task	Pearson r	Spearman r
GPT-5.2 [28]	Basic Grounding	0.6661	0.6216
GPT-5.2 [28]	Complex Grounding	0.2595	0.3201
Qwen3-VL-8B [4]	Basic Grounding	0.2796	0.5212
Qwen3-VL-8B [4]	Complex Grounding	0.0902	0.1321
MAP-Agent	Basic Grounding	0.2533	0.4478
MAP-Agent	Complex Grounding	0.0278	0.1748

performance is measured by S_{box} . Fig. 4 visualizes the sample-level relationship between target side length and S_{box} , while Tab. 16 reports Pearson and Spearman correlations.

On *BG*, all models show positive correlations, indicating that larger targets are generally easier to localize. This effect is strongest for GPT-5.2, with Pearson $r = 0.6661$ and Spearman $r = 0.6216$. Together with the *BG* error diagnosis, this suggests that GPT-5.2 is highly sensitive to target scale in native UHR scenes: when the target becomes small relative to the full image canvas, the model often fails to discover valid object evidence and instead produces object hallucinations.

Qwen3-VL-8B exhibits a weaker linear dependence on target size than GPT-5.2 on *BG* (Pearson $r = 0.2796$), although its Spearman correlation remains moderate ($r = 0.5212$). This indicates that Qwen3-VL-8B is less dominated by target size in absolute score variation, but target scale still affects the rank ordering of localization difficulty. MAP-Agent further reduces both correlations on *BG* compared with the Qwen3-VL-8B baseline (Pearson $r = 0.2533$, Spearman $r = 0.4478$), suggesting that localized ROI inspection slightly weakens the model’s dependence on target size and improves evidence acquisition beyond simply favoring larger or more salient targets.

On *CG*, correlations are substantially weaker for all models. GPT-5.2 still shows a modest positive relationship between target size and performance, whereas Qwen3-VL-8B and MAP-Agent show only weak correlations. In particular, MAP-Agent has an almost negligible Pearson correlation on *CG* ($r = 0.0278$), although its Spearman correlation remains slightly positive ($r = 0.1748$). This suggests that once multi-hop spatial or relational constraints are introduced, target size alone no longer explains localization performance. Complex grounding depends more strongly on region selection, contextual interpretation, and distinguishing the correct instance among nearby distractors. Therefore, target scale is a major factor for basic grounding, while complex grounding is governed by a broader combination of scale, context, and relational reasoning.

Overall, the scale analysis shows that target size is a key driver of basic grounding performance, especially for GPT-5.2 in native UHR scenes. However, the weaker correlations on complex grounding indicate that scale is not the only source of difficulty: once relational and contextual constraints are introduced, successful localization also requires reliable region selection and context-consistent target identification.

E.4 Coordinate Format Robustness

Finally, we evaluate whether VLM localization performance is sensitive to the coordinate convention used in the prompt. This experiment is motivated by the fact that UHR images naturally involve large absolute pixel coordinates, while VLMs may have different numerical grounding behaviors under normalized coordinate systems. As a diagnostic study, we compare three coordinate formats: a 1000-base coordinate system, a unit-scale coordinate system, and absolute pixel coordinates. In the 1000-base format, both axes are scaled to $[0, 1000]$. In the unit-scale format, coordinates are scaled to $[0, 1]$. In the absolute format, coordinates are expressed in the original image pixel space.

We evaluate GPT-5.2, Qwen3-VL-8B, and InternVL3.5-8B under otherwise identical prompts and image-query pairs. Predictions from all coordinate formats are converted back to the original absolute-pixel image coordinate system before scoring, ensuring that performance differences reflect coordinate-format robustness rather than metric differences.

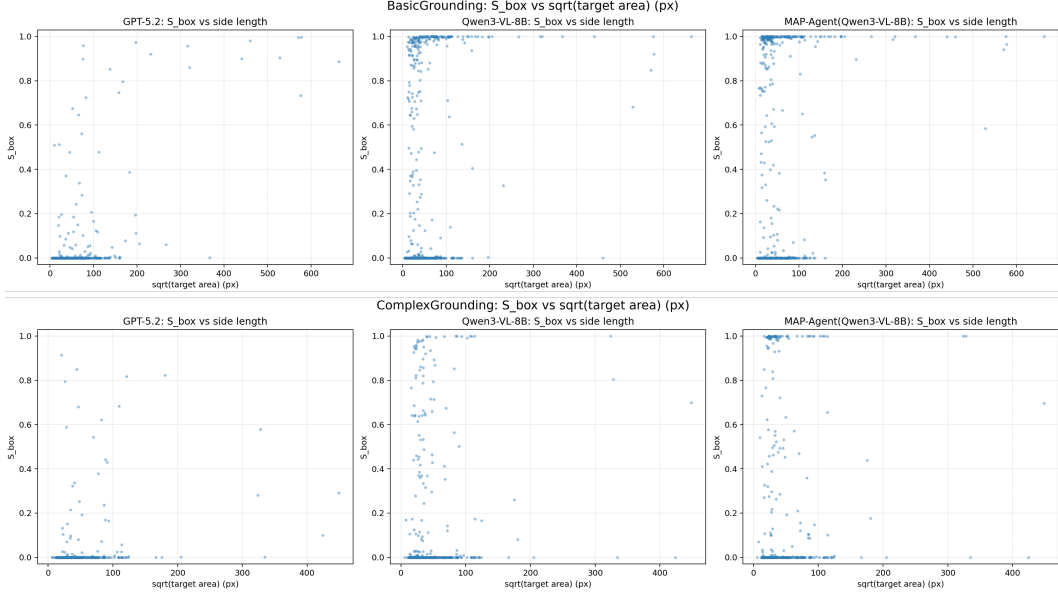


Figure 4: Relationship between target side length and localization score S_{box} on *Basic Grounding* (BG) and *Complex Grounding* (CG). Each point corresponds to one grounding sample, and results are shown for GPT-5.2, Qwen3-VL-8B, and MAP-Agent. The scatter plots show that target size has a strong effect on BG, especially for GPT-5.2, while the relationship becomes weaker on CG where contextual and relational constraints dominate.

Table 17: Coordinate format robustness. All predictions are converted back to the original absolute-pixel image coordinate system before evaluation.

Model	1000-base Coordinates	Unit-scale Coordinates	Absolute Pixel Coordinates
GPT-5.2	3.34	2.06	3.12
Qwen3-VL-8B	24.54	5.46	0
InternVL3.5-8B	3.32	0	0

As shown in Tab. 17, the 1000-base coordinate format is the most robust choice across models. Qwen3-VL-8B shows a large performance gap between 1000-base coordinates and the other two formats, dropping from 24.54 to 5.46 under unit-scale coordinates and to 0 under absolute pixel coordinates. InternVL3.5-8B also fails under unit-scale and absolute coordinates, while retaining non-zero performance under the 1000-base format. GPT-5.2 is less sensitive to the choice of coordinate convention, but its overall localization performance remains low across all formats.

These results suggest that coordinate convention is not merely a formatting detail in UHR localization. Although UHR-Micro stores ground-truth annotations in absolute pixel coordinates, directly requiring VLMs to emit large image-dependent coordinates may conflate visual localization ability with numerical-format difficulty. Unit-scale coordinates introduce the opposite problem by compressing spatial differences into small decimals. The 1000-base coordinate system provides a more stable benchmarking interface, allowing VLMs to express spatial predictions more reliably while still preserving sufficient localization precision. Therefore, we adopt 1000-base coordinates as the default model-output format for benchmarking, while allowing models or APIs with a defined native coordinate convention to use that convention when applicable. All predictions are converted back to absolute pixel coordinates before scoring against the original annotations.

F Qualitative Examples of UHR-Micro

This section presents qualitative examples from UHR-Micro to illustrate the diversity of task formulations, visual conditions, answer formats, and model behaviors. We provide one representative example for each of the 16 tasks in the benchmark, as shown in Fig. 5–20. Each example contains the UHR image or the relevant visual crop, the natural-language instruction, the ground-truth answer,

and predictions from representative models. These examples complement the quantitative results by showing how micro-target perception failures arise in realistic UHR scenes.

G Datasheets

G.1 Motivation

1. *“For what purpose was the dataset created?”*

A: UHR-Micro was created to address the lack of systematic benchmarks for evaluating micro-target perception in ultra-high-resolution Earth observation imagery. Existing multimodal remote sensing benchmarks primarily emphasize scene-level semantics, salient objects, or cropped image patches, leaving it unclear whether vision–language models can locate and reason over extremely small but task-critical visual evidence within native UHR scenes. UHR-Micro fills this gap by providing a diagnostic evaluation suite with deterministic instructions across grounding, fine-grained understanding, counting, and spatial reasoning tasks. The dataset is designed to expose the scale disparity between tiny targets and massive image canvases, operationalize the resulting resolution illusion, and support controlled analysis of failure modes such as missed localization, hallucination, and coordinate shift. Overall, UHR-Micro aims to facilitate the development and rigorous benchmarking of perception-aware VLMs capable of reliable global-to-local reasoning in real-world UHR imagery.

2. *“Who created the dataset (e.g., which team, research group) and on behalf of which entity?”*

A: The dataset was created by the following authors:

- Anonymous authors

3. *“Who funded the creation of the dataset?”*

A: The dataset creation was funded by the affiliations of the authors involved in this work.

G.2 Composition

Most of the questions in this section are intended to provide dataset consumers with the information they need to make informed decisions about using the dataset for their chosen tasks. Some of the questions are designed to elicit information about compliance with the EU’s General Data Protection Regulation (GDPR) or comparable regulations in other jurisdictions. Questions that apply only to datasets that relate to people are grouped together at the end of the section. We recommend taking a broad interpretation of whether a dataset relates to people. For example, any dataset containing text that was written by people relates to people.

1. *“What do the instances that comprise our datasets represent (e.g., documents, photos, people, countries)?”*

A: The dataset primarily consists of remote sensing images captured by satellites and drones, along with task-specific textual annotations. The source datasets used in UHR-Micro are publicly released remote sensing datasets; UHR-Micro preserves source attribution and follows the corresponding source licenses and terms.

2. *“How many instances are there in total (of each type, if appropriate)?”*

A: UHR-Micro includes 11,253 instructions over 1,212 UHR images. Details can be found in the main text.

3. *“Does the dataset contain all possible instances or is it a sample (not necessarily random) of instances from a larger set?”*

A: The images in UHR-Micro are sourced from existing detection and segmentation datasets. All textual annotations were independently created by us.

4. *“Is there a label or target associated with each instance?”*

A: Yes. Each instance contains an image, an instruction, and a deterministic target answer.

5. *“Is any information missing from individual instances?”*

A: No, each individual instance is complete.

6. “*Are relationships between individual instances made explicit (e.g., users’ movie ratings, social network links)?*”

A: Yes. Each instruction is associated with its source image and task-specific target annotations; no social or user-level relationships are included.
7. “*Are there recommended data splits (e.g., training, development/validation, testing)?*”

A: Yes, UHR-Micro provides development, validation, and test query splits.
8. “*Is the dataset self-contained, or does it link to or otherwise rely on external resources (e.g., websites, tweets, other datasets)?*”

A: UHR-Micro will be released with processed images, annotations, source metadata, and usage documentation on platforms such as GitHub and Hugging Face, subject to the licenses and terms of the underlying source datasets.
9. “*Does the dataset contain data that might be considered confidential (e.g., data that is protected by legal privilege or by doctor–patient confidentiality, data that includes the content of individuals’ non-public communications)?*”

A: To the best of our knowledge, UHR-Micro does not contain confidential records, private communications, or medical, financial, or legal records. The images are derived from publicly released remote sensing datasets, and annotations are constructed for benchmark evaluation.
10. “*Does the dataset contain data that, if viewed directly, might be offensive, insulting, threatening, or might otherwise cause anxiety?*”

A: UHR-Micro does not intentionally include offensive, insulting, or graphic content. However, as an Earth observation benchmark, it may contain publicly observable infrastructure, vehicles, vessels, or facilities, and should therefore be used with appropriate awareness of dual-use risks.

G.3 Collection Process

In addition to the goals outlined in the previous section, the questions in this section are designed to elicit information that may help researchers and practitioners create alternative datasets with similar characteristics. Again, questions that apply only to datasets that relate to people are grouped together at the end of the section.

1. “*How was the data associated with each instance acquired?*”

A: The images in UHR-Micro are sourced from existing public remote sensing detection and segmentation datasets, and we enrich them with task-specific textual instructions and target answers. Details are provided in Section 3 of the main text.
2. “*What mechanisms or procedures were used to collect the data (e.g., hardware apparatuses or sensors, manual human curation, software programs, software APIs)?*”

A: UHR-Micro was constructed by curating images and annotations from established public remote sensing datasets. No additional hardware apparatuses, sensors, or image acquisition campaigns were introduced. We first filtered source images to retain 4K-scale ultra-high-resolution scenes with sufficient dense object annotations. Based on these native UHR images and their ground-truth annotations, we built a three-tier hybrid data engine. First, foundational tasks driven by coordinate, category, counting, and spatial-relation mappings were generated programmatically using geometric rules and existing dense annotations. Second, tasks requiring descriptive semantic alignment, such as basic grounding and pattern distribution recognition, were generated with the assistance of a frontier vision–language model through API-based prompting and then cross-validated by human annotators. Third, tasks involving complex multi-hop spatial reasoning, including complex grounding, cross-region comparative counting, and multi-condition retrieval, were constructed under a human-led protocol by domain experts, with model assistance used only as auxiliary support. All candidate samples were subjected to format validation, target-existence checks, ambiguity filtering, and expert review where necessary to ensure deterministic and unambiguous evaluation targets.
3. “*If the dataset is a sample from a larger set, what was the sampling strategy (e.g., deterministic, probabilistic with specific sampling probabilities)?*”

A: Please refer to the details listed in the main text Section 3.

G.4 Preprocessing, Cleaning, and Labeling

The questions in this section are intended to provide dataset consumers with the information they need to determine whether the “raw” data has been processed in ways that are compatible with their chosen tasks. For example, text that has been converted into a “bag-of-words” is not suitable for tasks involving word order.

1. *“Was any preprocessing/cleaning/labeling of the data done (e.g., discretization or bucketing, tokenization, part-of-speech tagging, SIFT feature extraction, removal of instances, processing of missing values)?”*

A: Yes. UHR-Micro involved preprocessing, cleaning, and labeling steps to ensure that all samples support deterministic evaluation. During preprocessing, source annotations from different remote sensing datasets were converted into a unified format, and 4K-scale UHR images with valid dense object annotations were retained. Corrupted images, incomplete annotations, ambiguous targets, and samples whose answers could not be deterministically verified were removed. For task construction, existing object annotations were transformed into task-specific labels, including bounding boxes, segmentation masks, numerical answers, and discrete options. Coordinate-based tasks, counting tasks, and spatial-relation tasks were generated through rule-based geometric processing, while semantically richer tasks were labeled through VLM-assisted generation followed by human verification or expert-led annotation. All instructions and answers were further checked for format consistency, target existence, duplicate or near-duplicate cases, and ambiguity before being included in the final development, validation, and test splits.

2. *“Was the ‘raw’ data saved in addition to the preprocessed/cleaned/labeled data (e.g., to support unanticipated future uses)?”*

A: Yes. The underlying source images and annotations remain accessible through their original public dataset releases, subject to their respective licenses and terms.

3. *“Is the software that was used to preprocess/clean/label the data available?”*

A: Yes. The preprocessing and evaluation scripts will be made publicly available with the benchmark release.

G.5 Uses

The questions in this section are intended to encourage dataset creators to reflect on tasks for which the dataset should and should not be used. By explicitly highlighting these tasks, dataset creators can help dataset consumers make informed decisions, thereby avoiding potential risks or harms.

1. *“Has the dataset been used for any tasks already?”*

A: Yes. It is used in this paper to benchmark micro-target perception and global-to-local reasoning in VLMs.

2. *“Is there a repository that links to any or all papers or systems that use the dataset?”*

A: Yes. We will provide such links on the project GitHub and Hugging Face repositories.

3. *“What (other) tasks could the dataset be used for?”*

A: Beyond benchmarking micro-target perception in VLMs, UHR-Micro can support research on high-resolution object detection, referring expression grounding, fine-grained remote sensing recognition, dense object counting, spatial relationship reasoning, active visual search, and agentic global-to-local perception.

4. *“Is there anything about the composition of the dataset or the way it was collected and preprocessed/cleaned/labeled that might impact future uses?”*

A: No.

5. *“Are there tasks for which the dataset should not be used?”*

A: UHR-Micro should not be used for privacy-invasive monitoring, operational surveillance, targeting, or safety-critical decision-making without appropriate validation, authorization, and human oversight.

G.6 Distribution

Dataset creators should provide answers to these questions prior to distributing the dataset either internally within the entity on behalf of which the dataset was created or externally to third parties.

1. *“Will the dataset be distributed to third parties outside of the entity (e.g., company, institution, organization) on behalf of which the dataset was created?”*
A: The benchmark will be made publicly accessible to the research community, subject to the licenses and terms of the underlying source datasets.
2. *“How will the dataset be distributed (e.g., tarball on website, API, GitHub)?”*
A: We will provide UHR-Micro in the GitHub and the Hugging face repository.
3. *“When will the dataset be distributed?”*
A: We will create a repository to release the data once the paper is officially published.
4. *“Will the dataset be distributed under a copyright or other intellectual property (IP) license, and/or under applicable terms of use (ToU)?”*
A: Yes. The newly created UHR-Micro instructions, annotations, and metadata will be released under the Creative Commons Attribution-NonCommercial-ShareAlike 4.0 International License, while source imagery remains subject to the licenses and terms of the original datasets.
5. *“Have any third parties imposed IP-based or other restrictions on the data associated with the instances?”*
A: Yes. The underlying source images are subject to the licenses and terms of their original datasets. UHR-Micro will preserve source attribution and document applicable usage constraints in the release.
6. *“Do any export controls or other regulatory restrictions apply to the dataset or to individual instances?”*
A: We are not aware of export-control restrictions specific to UHR-Micro beyond the licenses and terms of the underlying source datasets. Users are responsible for ensuring compliance with applicable local regulations.

G.7 Maintenance

As with the questions in the previous section, dataset creators should provide answers to these questions prior to distributing the dataset. The questions in this section are intended to encourage dataset creators to plan for dataset maintenance and communicate this plan to dataset consumers.

1. *“Who will be supporting/hosting/maintaining the dataset?”*
A: The authors of this work will support, host, and maintain the dataset.
2. *“How can the owner/curator/manager of the dataset be contacted (e.g., email address)?”*
A: They can be contacted via the email addresses listed on the paper or webpage.
3. *“Is there an erratum?”*
A: There is no erratum for the initial release; updates and known issues will be documented on the project repository.
4. *“Will the dataset be updated (e.g., to correct labeling errors, add new instances, delete instances)?”*
A: Future updates (if any) will be posted on the dataset website.
5. *“Will older versions of the dataset continue to be supported/hosted/maintained?”*
A:
Yes. Older versions will be archived when feasible, and updates will be documented on the project repository.
6. *“If others want to extend/augment/build on/contribute to the dataset, is there a mechanism for them to do so?”*
A: Yes, we will provide detailed instructions for future extensions.

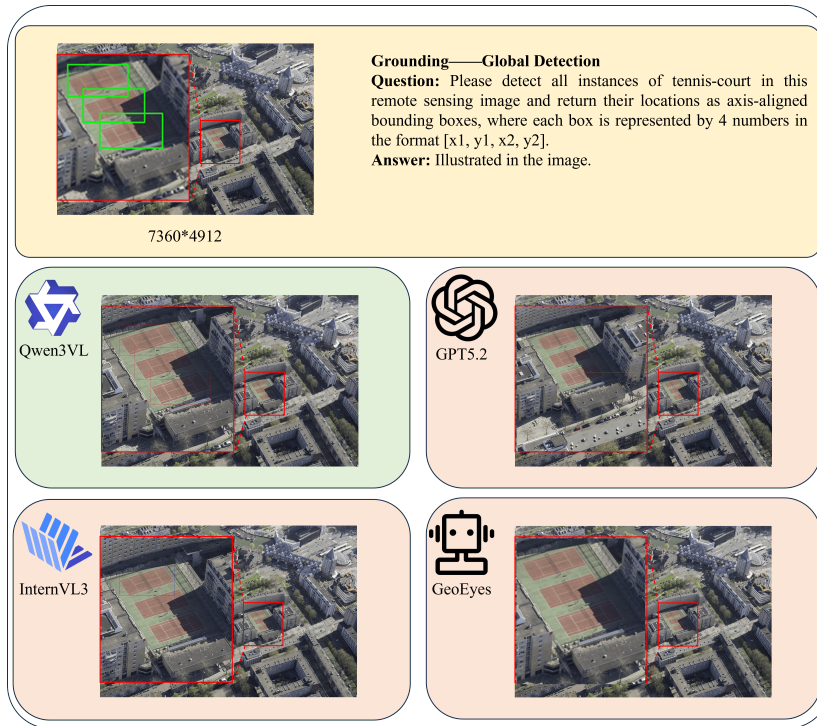


Figure 5: Example of *Global Detection (GD)*. The figure shows the UHR image, instruction, ground-truth, and model predictions.

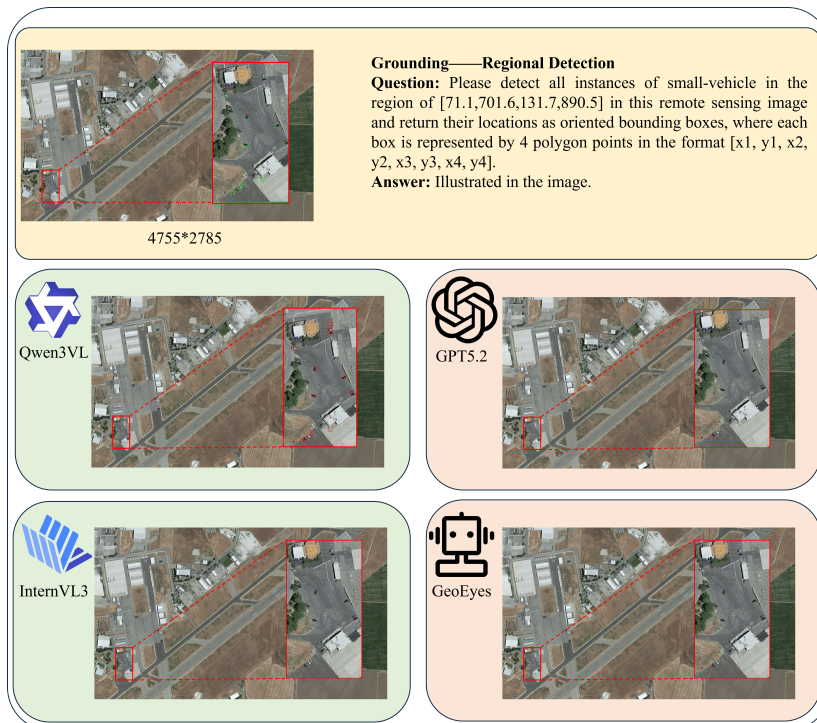


Figure 6: Example of *Regional Detection (RD)*. The figure shows the UHR image, instruction, ground-truth, and model predictions.

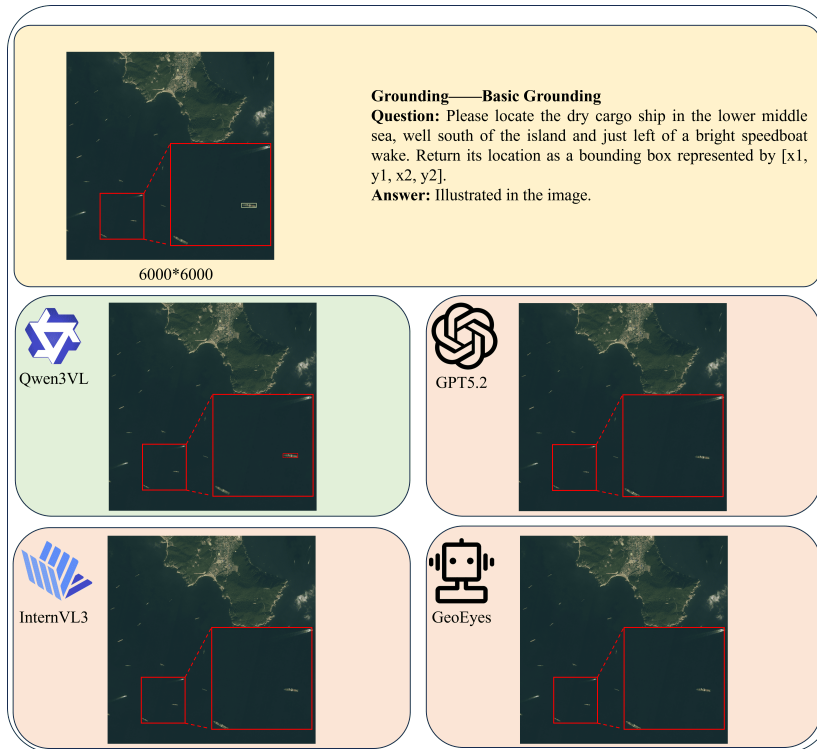


Figure 7: Example of *Basic Grounding (BG)*. The figure shows the UHR image, instruction, ground-truth, and model predictions.



Figure 8: Example of *Complex Grounding (CG)*. The figure shows the UHR image, instruction, ground-truth, and model predictions.

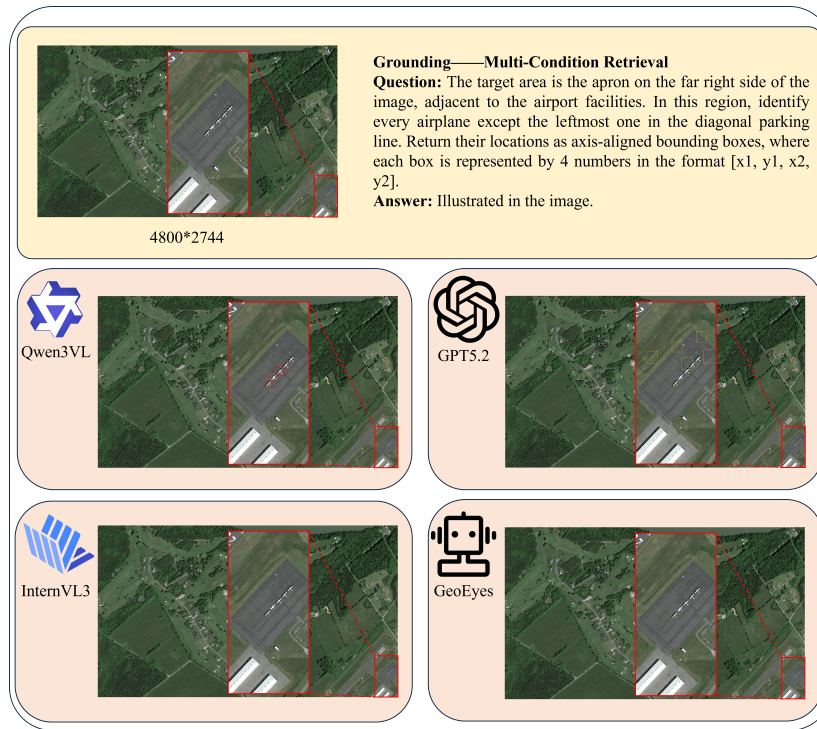


Figure 9: Example of *Multi-Condition Retrieval (MCR)*. The figure shows the UHR image, instruction, ground-truth, and model predictions.

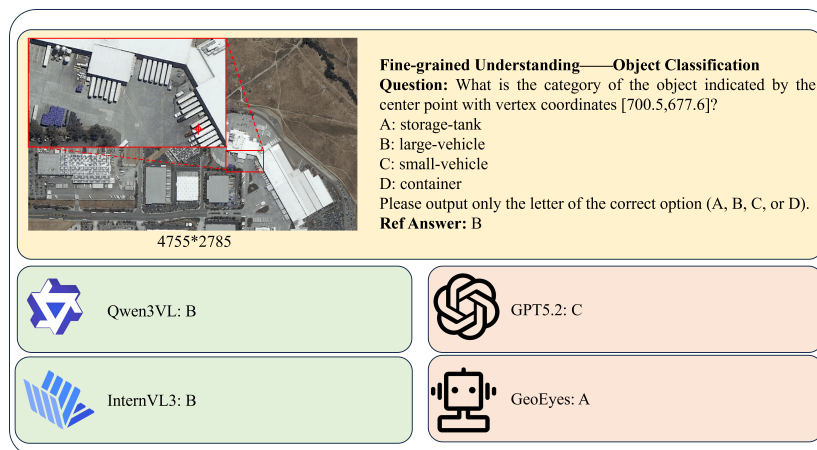


Figure 10: Example of *Object Classification (OC)*. The figure shows the UHR image, instruction, ground-truth, and model predictions.

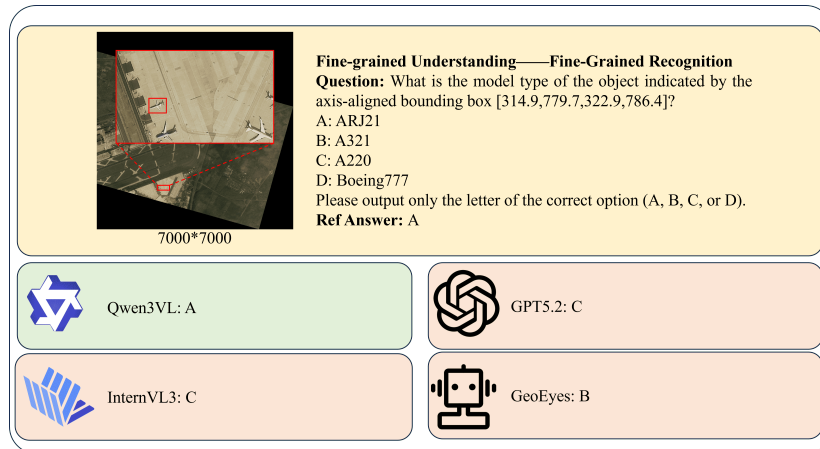


Figure 11: Example of *Fine-Grained Recognition (FGR)*. The figure shows the UHR image, instruction, ground-truth, and model predictions.

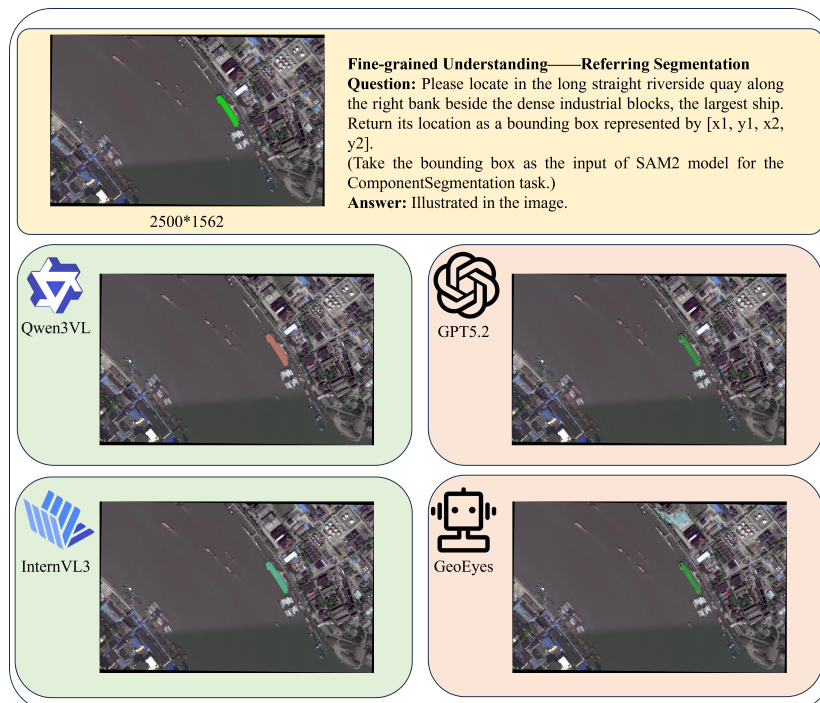


Figure 12: Example of *Referring Segmentation (RS)*. The figure shows the UHR image, instruction, ground-truth, and model predictions.

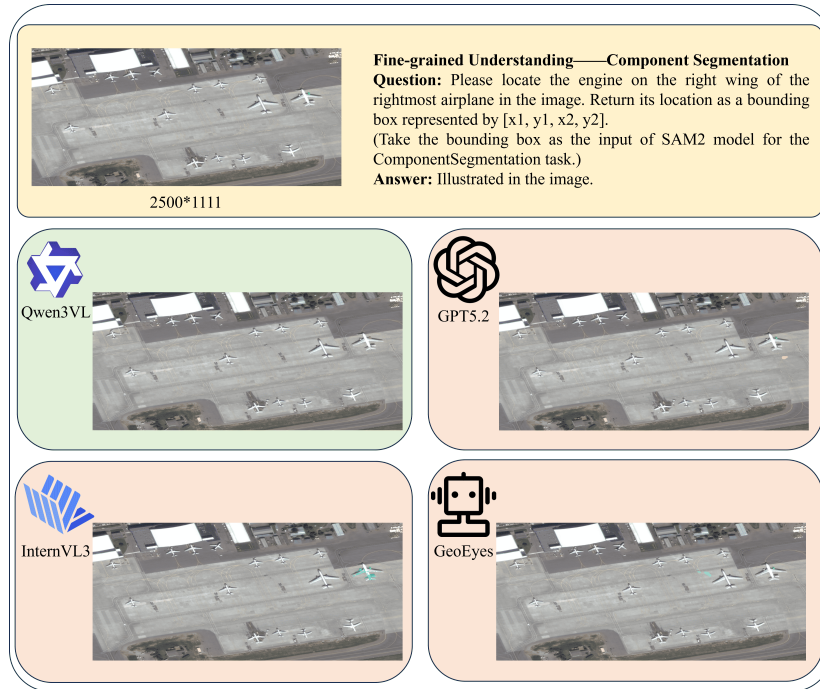


Figure 13: Example of *Component Segmentation (CS)*. The figure shows the UHR image, instruction, ground-truth, and model predictions.

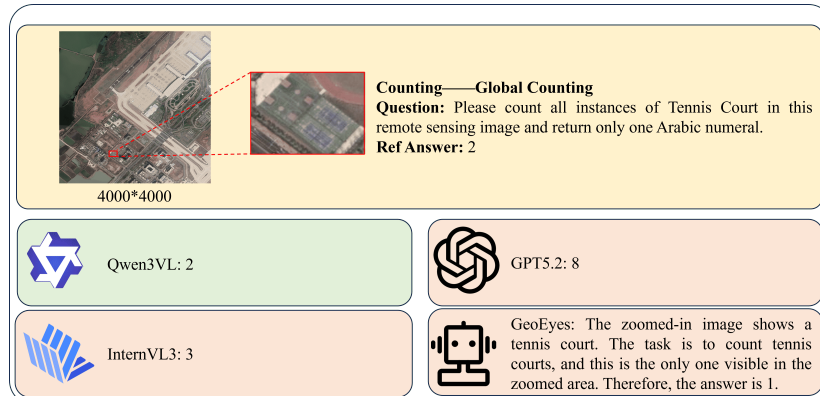


Figure 14: Example of *Global Counting (GC)*. The figure shows the UHR image, instruction, ground-truth, and model predictions.

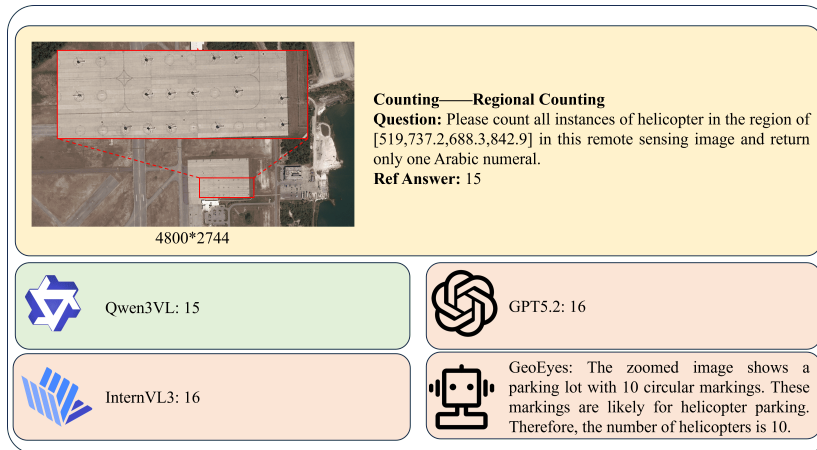


Figure 15: Example of *Regional Counting (RC)*. The figure shows the UHR image, instruction, ground-truth, and model predictions.

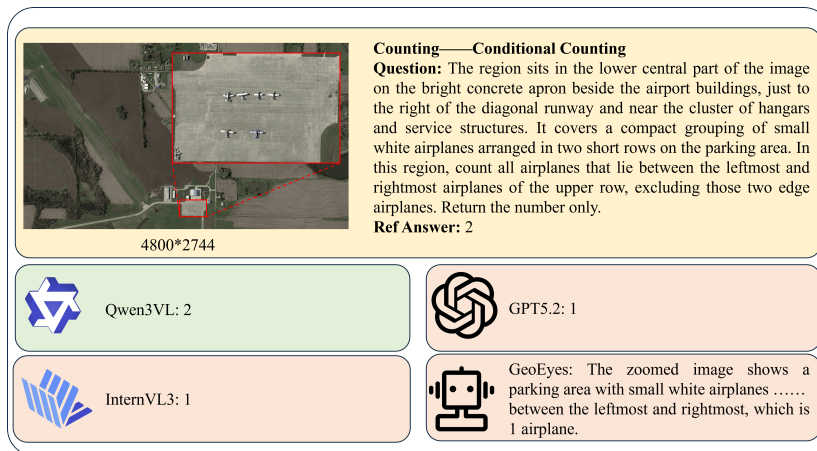


Figure 16: Example of *Conditional Counting (CC)*. The figure shows the UHR image, instruction, ground-truth, and model predictions.

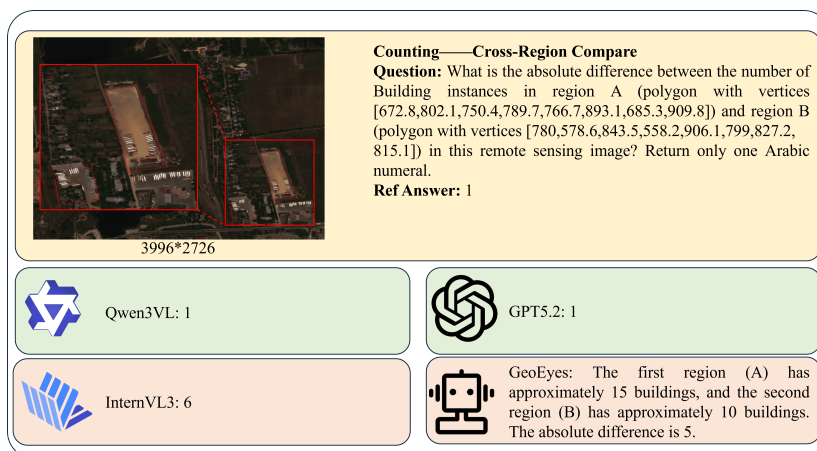
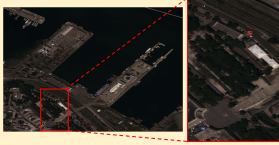




Figure 17: Example of *Cross-Region Compare (CRC)*. The figure shows the UHR image, instruction, ground-truth, and model predictions.




4541*2456

Spatial Reasoning—Directional Relationship
Question: Relative to the object in the blue box, in which direction is the object in the red box?
Choose one:
A. Northeast
B. Northwest
C. Southwest
D. Southeast
Ref Answer: A


Qwen3VL: A


GPT5.2: C


InternVL3: C


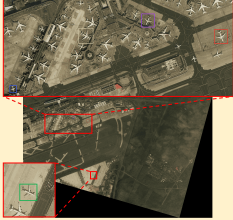


GeoEyes: C


Figure 18: Example of *Directional Relationship (DrR)*. The figure shows the UHR image, instruction, ground-truth, and model predictions.




7000*7000

Spatial Reasoning—Distance Relationship
Question: A reference object is marked with a red rectangle. Four other objects are marked with blue, green, yellow, and purple rectangles (one color per object). Which candidate object is spatially closest to the reference object marked with a red rectangle? Choose one:
A. The blue box
B. The green box
C. The yellow box
D. The purple box
Please output only the letter of the correct option (A, B, C, or D).
Ref Answer: D


Qwen3VL: D


GPT5.2: C


InternVL3: B


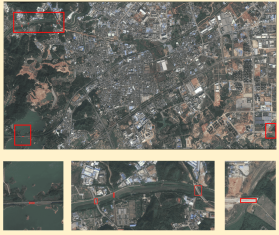


GeoEyes: C


Figure 19: Example of *Distance Relationship (DsR)*. The figure shows the UHR image, instruction, ground-truth, and model predictions.




4541*2456

Spatial Reasoning—Pattern Distribution Recognition
Question: The aerial image shows all instances of the target category "bridge" outlined in red. Which description best matches the spatial distribution of bridge targets in the image?
A. Top-right cluster; dense bottom-left band; scattered throughout residential areas.
B. Vertical distribution along waterway; concentration in upper half; gradual thinning southward.
C. Scattered across frame; dense cluster center-lower; right edge concentration; sparse upper-left.
D. Upper-left cluster; isolated lower-right corner instance.
Please output only the letter of the correct option (A, B, C, or D).
Ref Answer: D


Qwen3VL: D


GPT5.2: B


InternVL3: C



GeoEyes: C

Figure 20: Example of *Pattern Distribution Recognition (PDR)*. The figure shows the UHR image, instruction, ground-truth, and model predictions.